OPEN ACCESS

Original research

Accurate liquid biopsy for the diagnosis of non-alcoholic steatohepatitis and liver fibrosis

Giulia Angelini,[1,2] Simona Panunzi,[3] Lidia Castagneto-Gissey,[4] Francesca Pellicanò,[3] Andrea De Gaetano,[3] Maurizio Pompili,[1,2] Laura Riccardi,[2] Matteo Garcovich,[2] Marco Raffaelli,[1,2] Luigi Ciccoritti,[2] Ornella Verrastro,[1] Maria Francesca Russo,[1] Fabio Maria Vecchio,[1,5] Giovanni Casella,[4] James Casella-Mariolo,[6] Luigi Papa,[6] Pier Luigi Marini,[6] Francesco Rubino,[7] Carel W le Roux,[8] Stefan Bornstein,[9,10] Geltrude Mingrone [1,2,10]

► Additional supplemental material is published online only. To view, please visit the journal online (http://dx.doi.org/10.1136/gutjnl-2022-327498).

For numbered affiliations see end of article.

Correspondence to
Professor Geltrude Mingrone, Department of Medical and Surgical Sciences, Universita Cattolica del Sacro Cuore, Rome, Italy;
geltrude.mingrone@unicatt.it

GA and SP are joint first authors.

Received 1 April 2022
Accepted 30 June 2022

To cite: Angelini G, Panunzi S, Castagneto-Gissey L, *et al*. *Gut* Epub ahead of print: [*please include* Day Month Year]. doi:10.1136/gutjnl-2022-327498

ABSTRACT

Objective Clinical diagnosis and approval of new medications for non-alcoholic steatohepatitis (NASH) require invasive liver biopsies. The aim of our study was to identify non-invasive biomarkers of NASH and/or liver fibrosis.

Design This multicentre study includes 250 patients (discovery cohort, n=100 subjects (Bariatric Surgery Versus Non-alcoholic Steato-hepatitis - BRAVES trial); validation cohort, n=150 (Liquid Biopsy for NASH and Liver Fibrosis - LIBRA trial)) with histologically proven non-alcoholic fatty liver (NAFL) or NASH with or without fibrosis. Proteomics was performed in monocytes and hepatic stellate cells (HSCs) with iTRAQ-nano- Liquid Chromatography - Mass Spectrometry/Mass Spectrometry (LC-MS/MS), while flow cytometry measured perilipin-2 (PLIN2) and RAB14 in peripheral blood $CD14^{+}CD16^{-}$ monocytes. Neural network classifiers were used to predict presence/absence of NASH and NASH stages. Logistic bootstrap-based regression was used to measure the accuracy of predicting liver fibrosis.

Results The algorithm for NASH using PLIN2 mean florescence intensity (MFI) combined with waist circumference, triglyceride, alanine aminotransferase (ALT) and presence/absence of diabetes as covariates had an accuracy of 93% in the discovery cohort and of 92% in the validation cohort. Sensitivity and specificity were 95% and 90% in the discovery cohort and 88% and 100% in the validation cohort, respectively. The area under the receiver operating characteristic (AUROC) for NAS level prediction ranged from 83.7% (CI 75.6% to 91.8%) in the discovery cohort to 97.8% (CI 95.8% to 99.8%) in the validation cohort. The algorithm including RAB14 MFI, age, waist circumference, high-density lipoprotein cholesterol, plasma glucose and ALT levels as covariates to predict the presence of liver fibrosis yielded an AUROC of 95.9% (CI 87.9% to 100%) in the discovery cohort and 99.3% (CI 98.1% to 100%) in the validation cohort, respectively. Accuracy was 99.25%, sensitivity 100% and specificity 95.8% in the discovery cohort and 97.6%, 99% and 89.6% in the validation cohort. This novel biomarker was superior to currently used FIB4, non-alcoholic fatty liver disease fibrosis score and aspartate aminotransferase (AST)-to-platelet ratio and was comparable to ultrasound two-dimensional shear wave elastography.

Conclusions The proposed novel liquid biopsy is accurate, sensitive and specific in diagnosing the presence and severity of NASH or liver fibrosis and is more reliable than currently used biomarkers.

Clinical trials Discovery multicentre cohort: Bariatric Surgery versus Non-Alcoholic Steatohepatitis, BRAVES, ClinicalTrials.gov identifier: NCT03524365. Validation multicentre cohort: Liquid Biopsy for NASH and Fibrosis, LIBRA, ClinicalTrials.gov identifier: NCT04677101.

WHAT IS ALREADY KNOWN ON THIS TOPIC

⇒ The diagnosis of non-alcoholic steatohepatitis (NASH) currently relies on invasive liver biopsy. There is therefore an urgent need to find non-invasive biomarkers for NASH diagnosis, disease progression and intervention response monitoring. However, until now, no specific biomarker has been officially endorsed by the Food and Drug Administration and European Medicines Agency.

WHAT THIS STUDY ADDS

⇒ We identified two monocyte proteins, PLIN2 and RAB14, which are able to predict the presence and severity of NASH and liver fibrosis, respectively.

HOW THIS STUDY MIGHT AFFECT RESEARCH, PRACTICE OR POLICY

⇒ The biomarkers we identified are sensitive and specific in diagnosing the presence and severity of NASH and/or liver fibrosis and are more reliable than currently used biomarkers. A liquid biopsy is, therefore, feasible in making diagnosis of NASH and/or liver fibrosis. Sensitive and specific biomarkers can help in identifying patients eligible for NASH pharmacotherapy or surgery in clinical trials and treatment efficacy monitoring.

INTRODUCTION

The approval of drugs for non-alcoholic steatohepatitis (NASH) by the US Food and Drug Administration and the European Medicines Agency requires histological improvement of inflammation without worsening of fibrosis, or NASH resolution and fibrosis improvement.[1] Although histology remains the gold standard, the limitations include intraobserver and interobserver variability, but it also requires an invasive liver biopsy.

A large number of patients (65%–73%) enrolled in clinical trials who underwent liver biopsy do not meet the eligibility criteria.[2 3] Hence, prebiopsy strategies targeting the right candidates and reducing the number of screen failures are necessary. Indeed, the identification of appropriate biomarkers would increase patients' enrolment in clinical trials, accelerating the development of therapeutic interventions for NASH.

Unfortunately, plasma biomarkers for the diagnosis of NASH have low sensitivity, ranging from 62% to 66%, and specificity, between 78% and 82%.[4–17] Notably, none of the available biomarkers is able to predict the severity of NASH and, thus, NASH and fibrosis staging.

Moreover, it has been shown that scores of NASH and liver fibrosis greatly rely on body mass index (BMI) as a predictor variable and thus show a poor performance in obesity and morbid obesity with increase in false positives.[18]

Hence, we sought to identify a biomarker and algorithm able to predict not only the presence of NASH but also its severity.

We previously demonstrated that ectopic fat deposition in hepatocytes in non-alcoholic fatty liver (NAFL) and NASH correlates with ectopic fat accumulated in blood monocytes as lipid droplets (LDs).[19 20] Hepatic macrophages include not only resident Kupffer cells (KCs) but also monocyte-derived macrophages (MoMFs). It has been suggested that as far as NASH progresses, KCs are replaced by MoMFs.[21] These MoMFs can be reprogrammed or repolarised in the liver toward a proinflammatory and pathological phenotype acquiring a foamy phenotype. From the liver, they can re-enter the circulatory stream, as demonstrated in other diseases,[22] in a dynamic transition.

NAFLs/NASHs are often associated with liver fibrosis, representing the main determinant of mortality in NASH.[7 8] Liver fibrosis derives from the accumulation of extracellular matrix proteins. Inflammation activates KCs, releasing proinflammatory cytokines, including transforming growth factor beta-1. In turn, these activate transdifferentiation of hepatic stellate cells (HSCs) into myofibroblasts, the major source of extracellular matrix.[9 23 24]

The intracellular transport of metalloproteinases, HSCs enzymes that degrade collagen[25] and consequently their secretion are regulated by a set of Ras-related protein (RAB) GTPases, including RAB.[26]

Our study tested perilipin-2 (PLIN2) levels in circulating monocytes as a predictor of histological NASH. Secondary, we tested RAB14 levels in circulating monocytes as a predictor of liver fibrosis.

METHODS

Cohorts

Discovery cohort

The discovery cohort consisted of 100 consecutive subjects aged 46.9±10.5 years (67% women), screened during the enrolment of BRAVES (ClinicalTrials.gov identifier: NCT03524365), a multicentre randomised controlled trial (RCT) in which 288 subjects with histologically proven NASH with or without liver fibrosis were randomised (1:1:1) in three intervention arms (intensive lifestyle modification and medical treatment, Roux-en-Y gastric bypass (RYGB) or sleeve gastrectomy). Thirty-nine of the 100 subjects had screen failure after liver biopsy showing NAFL rather than NASH, and therefore they were excluded from the BRAVES trial.

The metabolic surgery cohort consisted of 50 different subjects enrolled in the BRAVES RCT studied at baseline and at 1 year after RYGB.

None of the subjects had secondary causes or a history of alcohol excess.

Enrolment inclusion criteria were liver ultrasound showing steatosis, non-alcoholic fatty liver disease (NAFLD) fibrosis score of >0.676, BMI of ≥30 and <50 kg/m^2 (amendment 1 July 2019, previously BMI ≤40 kg/m^2), age 25–65 years, both sexes, with informed consent signed.

Enrolment exclusion criteria were (1) regular and/or excessive alcohol uptake (>20 g alcohol/day for women and >30 g alcohol/day for men); (2) clinical evidence of NAFLD secondary to iatrogenic GI or immunodeficiency (HIV infection) diseases; (3) clinical evidence of non-NAFLD hepatic diseases, including hepatitis B or C, or haemochromatosis; (4) Wilson's disease; (5) glycogenosis; (6) alpha-1 antitrypsin deficiency; (7) autoimmune hepatitis; (8) cholestasis liver disease; (9) presence of relevant cardiovascular, GI or respiratory diseases, or any hormonal disorder; (10) clinical evidence of decompensated liver disease (Child-Pugh score >7 points); (11) undergoing narcotics abuse; (12) relevant systemic diseases; and (13) pregnancy.

Validation cohort

The validation cohort included 150 subjects (LIBRA study, ClinicalTrials.gov identifier: NCT04677101) aged 43.4±11.9 years, with 56% women. LIBRA, a multicentre cohort study, enrolled 100 individuals with histologically proven NASH with or without liver fibrosis and 50 individuals who underwent elective cholecystectomy and whose histology showed either NAFL or no histological lesions.

Inclusion criteria for the 100 subjects were NASH documented by liver biopsy and no evidence of another form of liver disease in subjects with a BMI of ≥30 and ≤55 kg/m^2. Fifty subjects, who underwent laparoscopic elective cholecystectomy but were otherwise in healthy conditions, aged 25–65 years, including both sexes, with informed consent signed, had an apparently normal liver.

Exclusion criteria were coronary event or procedure (myocardial infarction, unstable angina, coronary artery bypass and surgery or coronary angioplasty) in the previous 6 months; liver cirrhosis; end-stage renal failure; participation in any other concurrent therapeutic clinical trial; any other life-threatening, non-cardiac disease; pregnancy; inability to give informed consent; substantial alcohol consumption (>20 g/day for women or >30 g/day for men); Wilson's disease; lipodystrophy; parenteral nutrition; and interfering medications (eg, amiodarone, methotrexate, tamoxifen and corticosteroids).

The authors had full access to the data and take responsibility for the completeness and accuracy of the data and integrity of their analysis.

Liver biopsy and histology

In subjects with obesity, percutaneous liver biopsies were performed under ultrasonography with 16-gauge biopsy needles. Needle liver biopsies (also 16-gauge biopsy needles) were obtained during laparoscopic cholecystectomy. All liver biopsies had a length of >15 mm and contained ≥11 portal areas.[27]

NASH was diagnosed histologically in the presence of steatosis, lobular inflammation and hepatocyte ballooning with or without perisinusoidal fibrosis, and NASH activity was graded according to the value of Non-alcoholic Fatty Liver Disease Activity Score (NAS). NAS was calculated by adding the severity scores for steatosis, lobular inflammation and ballooning with a range from 0 to 8.[28] A NAS=3, resulting from the sum of steatosis=1, lobular inflammation=1 and hepatocyte ballooning=1, was the minimum value to make a diagnosis of NASH.[29]

The Steatosis, Activity, Fibrosis (SAF) score was also calculated.[30] Fibrosis, steatosis and activity were staged according to the system described by Kleiner *et al*[29] and Brunt *et al*.[31]

The SAF scoring system separately assesses the grade of steatosis S histologically from S0 to S3, the activity grade A from A0 to A4 by addition of grades of ballooning and lobular inflammation, each graded from 0 to 2, and the stage of fibrosis F, from F0 to F4 according to NASH clinical research network (CRN) staging system. A single expert pathologist (FMV) read in a blinded manner the digitised slides according to CRN criteria. Relecture of the histological scores on digitalised images by a second independent pathologist (JCM) was performed.

Elastography

All patients underwent two-dimensional shear wave elastography, performed with MyLab V.9 platform ultrasound system (Esaote, Genova, Italy) using a convex broadband abdominal probe C1-8 MHz. Liver stiffness was measured obtaining four valid measurements in each patient considering both the median values in kilopascal and the ratio between IQR and the median value (M) (directly provided by the software) for the analysis. This technique has been shown to be effective in differentiating significant fibrosis ≥F2 from mild or absent fibrosis in a large series of patients with compensated chronic liver disease without comorbidities potentially affecting liver stiffness measurement.[32] The cut-off thresholds used to stage fibrosis are reported in Garcovich *et al*.[32]

Online supplemental materials report the methods for anthropometric measures, dual X-ray absorptiometry, blood sample analyses, proteomic, human primary hepatocyte isolation, human primary HSC isolation, cell viability and cell purity after isolation, isolation of peripheral blood mononuclear cells, immunofluorescence, flow cytometry, and validation parameters and more detailed statistics.

Statistical methods

Sample size was calculated based on a restrictive hypothesis of area under the receiver operating characteristic (AUROC)=0.70 for the new diagnostic test in discriminating subjects with and without NASH. We used a one-sided test: H0: AUROC=0.5, vs H1: AUROC >0.5, power=90%, alpha=0.025. The ratio between cases and controls was set at 0.6, and the total number of subjects enrolled in the discovery cohort was calculated as 84. Considering an attrition rate of 15%, we estimated a final sample size of 100 subjects (40 with NASH and 60 without) in the discovery cohort. The validation cohort was 3/2 of the discovery cohort, therefore 150 patients were enrolled. The software used was easyROC.[33]

The main outcome was the prediction of NASH diagnosis using a score derived from a neural network (NN) classifier including PLIN2 mean florescence intensity (MFI) in monocytes and ALT, presence/absence of diabetes, triglycerides and waist circumference as covariates. These covariates, with proven univariate model significance, represent hepatic function and metabolic and lipid profiles.

For SAF-A level prediction, see online supplemental tables 1 and 2.

Variables not normally distributed were log-transformed prior to analyses. Missing data were not replaced by imputation. In our machine-learning analysis, we combined NN-based probabilistic classification with resampling/bootstrapping. In this way, we calculated the number of hidden nodes and the analysis accuracy. The importance of variables was calculated using the Olden method.[34] Model discrimination was measured by the AUROC. AUROC CIs were computed by bootstrapping procedure.

The total NAS score, computed as the sum of scores for steatosis, lobular inflammation and ballooning, originally ranging from 0 to 8 was split into three levels: NAS level=0 for total NAS score of <3, NAS level=1 for total NAS score=3 and NAS level=2 for total NAS score of ≥4. A NN classifier analysis was used to predict NASH severity based on NAS scores. We calculated the confusion matrix, accuracy and receiver operating characteristic (ROC) curves, with the respective areas under the curve (AUCs), for each level of NAS.

RAB14 (MFI) was tested as predictor of liver fibrosis, diagnosed by SAF-F (presence: SAF-F ≥1, absence: SAF-F=0), in a multivariate logistic stepwise regression model including relevant covariates. Since in the discovery cohort only 3% of patients were free of fibrosis, according to SAF-F, making the dataset unsuitable for model development, we randomly split the whole dataset into a discovery and a validation set to obtain a balanced number of patients with and without fibrosis, using the createdataPartition function of the R caret package, which allows random split of the sample, preserving the overall class distribution of the data.

SAF-F was then recoded as a three-level variable: SAF-F_level=0 if SAF-F=0, SAF-F_level=1 if SAF-F=1 and SAF-F_level=2 if SAF-F is ≥2.

RAB14 was then used to predict SAF-F levels in a multinomial model. A model including elastography instead of RAB14 was also used to compare the predictive capacity of the two predictors. The quantitative variables were log-transformed prior to the analyses. AUROC assessed the discrimination ability of the model. The Youden criterion and the 'closest top-left' methods were employed to determine the best threshold. When Youden's J statistic is used, the optimal cut-off is the threshold that maximises the distance from the diagonal line or, in other words, that maximises the sum of the sensitivity and specificity. The closest top-left method instead determines the optimal threshold as the point closest to the top-left part of the plot with perfect sensitivity or specificity; specifically, it minimises the quantity $((1-\text{sensitivities})^2+(1-\text{specificities})^2)$. The two criteria may or may not lead to the same cut-off point, but while the Youden criterion reflects the intention of maximising overall correct classification rates, the closest top-left criterion mathematically involves a quadratic term of non-immediate interpretation from a clinical point of view.[35]

AUROCs of the new score and classical indices of fibrosis (NAFLD fibrosis score, FIB4 and AST-to-platelet ratio) were compared according to DeLong *et al*.[36]

Continuous variables are reported as mean and SD, while categorical variables are reported as numbers and percentages. A p value of <0.05 was considered statistically significant. The analyses were conducted in R.[37]

RESULTS

Proteomics and in vitro studies

To identify a possible biomarker of liver fibrosis, we performed proteomics in monocytes and HSCs obtained from liver biopsies of 5 subjects (2 men and 3 women) with NASH and liver fibrosis and in five subjects with negative histology for NASH and liver fibrosis from the LIBRA trial. Age was 45.80±6.18 in subjects with NASH and 40.60±2.41 years (p=0.118) in those without NASH; BMI was 39.21±6.22 and 36.20±4.76 kg/m^2 (p=0.415) in subjects with and without NASH, respectively.

Two of the subjects in each group had type 2 diabetes (T2D) and hypertension and were treated with metformin and Dipeptidyl Peptidase-IV (DPP-IV) inhibitors for diabetes and ACE inhibitors and beta blockers for hypertension.

Using p<0.0001 and q<0.0001 as statistical significance thresholds, the proteomic analysis identified nine proteins differentially expressed in both HSCs and monocytes. Ras-related protein Rab-18 (RAB18), annexin A6 (ANXA6) and Ras-related protein Rab-14 (RAB14) were downregulated, while disintegrin and metalloproteinase domain-containing proteins 8 and 9 (ADAM8 and ADAM9), Ras-related protein Rab-25 (RAB25), galectin-1 and 12 (LGALS1 and LGALS12) and profilin-1 (PFN1) were upregulated in the presence of liver fibrosis (see online supplemental figure 1). Among the proteins screened by proteomic, RAB14 was the most modified in the presence of fibrosis and our first choice as possible biomarker for the prediction of liver fibrosis.

To confirm the proteomic analysis, we have assessed RAB14 expression by flow cytometry in both monocytes and HSCs of 20 subjects with NASH and liver fibrosis and 20 subjects without NASH and liver fibrosis, spanning from normal liver to NAFL (figure 1A–E). A linear regression analysis confirmed a high correlation of RAB14 in monocytes and HSCs (R^2=0.73, p<0.0001) (figure 1F).

To assess PLIN2 as a possible diagnostic biomarker for NASH, we performed flow cytometry in monocytes and hepatocytes of the same subjects (figure 1G–K). Indeed, PLIN2 is a major protein coating LDs, and PLIN2 liver-specific knockout alleviates diet-induced hepatic steatosis and inflammation in mice.[38] Using flow cytometry analysis, we found a high correlation (R^2=0.85, p<0.0001) of PLIN2 expression in monocytes and hepatocytes (figure 1L).

The subjects included in RAB14 and PLIN2 analysis were 10 men and 10 women in each group, the mean age was 46.05±2.03 years in subjects with NASH and 43.80±1.79 years (p=0.411) in those without NASH; BMI was 38.49±1.23 and 35.97±0.87 kg/m^2 (p=0.103) in subjects with and without NASH, respectively. Ten subjects in each group had T2D and hypertension and were treated with Metformin, DPP-IV, and SGLT2i inhibitors for diabetes and ACE inhibitors and beta-blockers for hypertension.

Figure 1 shows the presence of LDs in monocytes and hepatocytes of two representative subjects, one with NASH/fibrosis (figure 1M–O) and the other one without NASH/fibrosis (figure 1N–P).

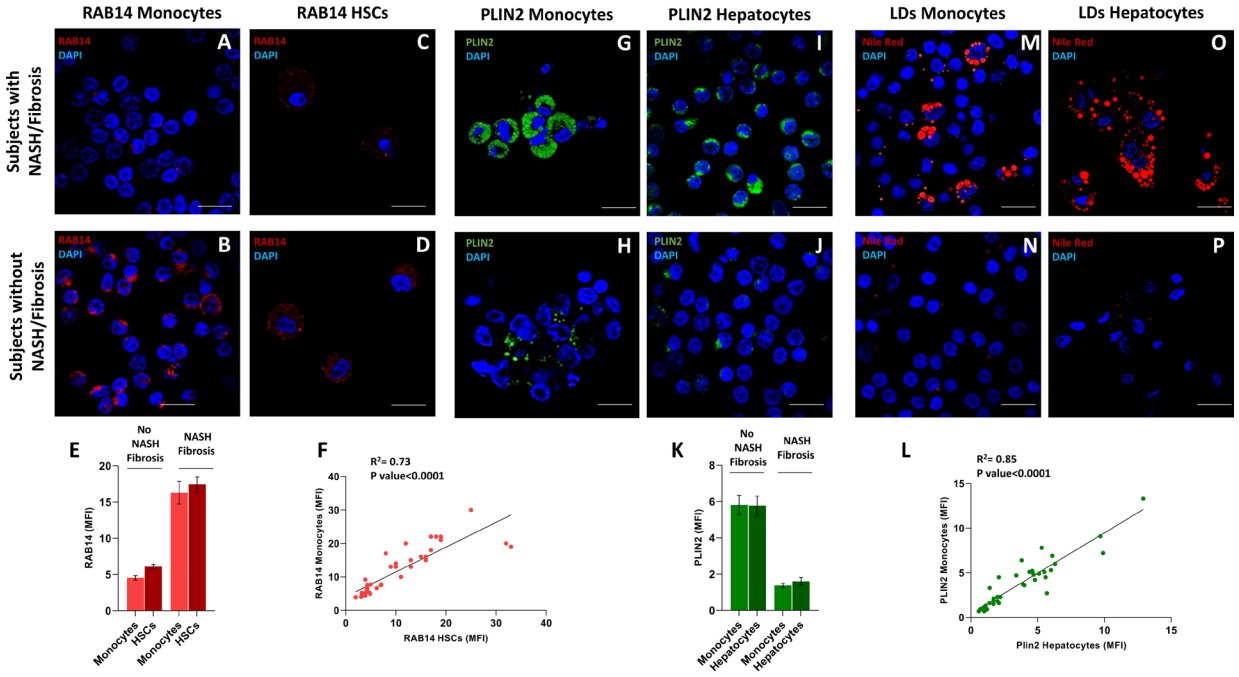

Figure 1 Laser scanning confocal immunofluorescence of monocytes, HSCs and hepatocytes from a representative subject with NASH/fibrosis (upper panels) and a representative subjects with negative histology for NASH/fibrosis (lower panels). (A–D) RAB14 staining in monocytes (A,B) and in HSCs (C,D). (E) Quantification of RAB14 protein expression by flow cytometry, in monocytes and HSCs of 20 subjects with NASH/fibrosis and 20 subjects with negative histology for NASH/fibrosis. (F) Spearman correlation analysis and linear regression line fitting of RAB14 expression in monocytes and HSCs. (G–J) PLIN2 staining in monocytes (G,H) and in hepatocytes (I,J). (K) Quantification of PLIN2 protein expression by flow cytometry in monocytes and hepatocytes of 20 subjects with NASH/fibrosis and 20 subjects with negative histology for NASH/fibrosis. (L) Spearman correlation analysis and linear regression line fitting of PLIN2 expression in monocytes and hepatocytes. (M–P) LDs staining with Nile Red in monocytes (M,N) and in hepatocytes (O,P). The mean NAS was 4.05±0.15 in the 20 subjects with NASH and liver fibrosis and 0.65±0.11 in the 20 subjects study without NASH and liver fibrosis from LIBRA. SAF-F mean was 1.95±0.17. Data are expressed as mean±SEM for linear regression analysis; Spearman rank correlation coefficients (R^2) and p values are shown. Magnification ×60. Scale bar: 50 µm. DAPI, 4', 6-Diamidino-2-Phenylindole; HSC, hepatic stellate cell; LD, lipid droplet; MFI, mean florescence intensity; NAS, Non-alcoholic Fatty Liver Disease Activity Score; NASH, non-alcoholic steatohepatitis; PLIN2, perilipin-2.

Table 1 Characteristics of the discovery, validation and whole cohorts

	Discovery 100 subjects		Validation 150 subjects		Whole 250 subjects		
Variable name	**Mean (SD)**	**(1st–3rd IQR)**	**Mean (SD)**	**(1st–3rd IQR)**	**Mean (SD)**	**(1st–3rd IQR)**	**P value**
Age	46.93 (10.54)	(40–54)	43.39 (11.91)	(33–53)	44.81 (11.49)	(36–53)	0.014
Weight (kg)	117.14 (22.07)	(103.5–130.25)	101.58 (31.98)	(75–124)	107.8 (29.39)	(88–126)	<0.001
Height (cm)	166.66 (9.13)	(160–172)	169.85 (9.85)	(162–178)	168.57 (9.68)	(161–176)	0.009
BMI (kg/m^2)	41.96 (5.86)	(38.53–46.03)	35.25 (10.72)	(23.1–42.43)	37.93 (9.66)	(32.74–44.27)	<0.001
Hip circumference (cm)	131.06 (14.1)	(120–142.5)	119.25 (21.69)	(99–135.25)	123.67 (20.01)	(110–138.5)	<0.001
Waist circumference (cm)	129.19 (17.57)	(115.75–143)	114 (26.22)	(87.04–134.75)	120.07 (24.28)	(104.25–137.88)	<0.001
Waist to hip ratio	0.98 (0.09)	(0.93–1.06)	0.96 (0.1)	(0.89–1.03)	0.97 (0.09)	(0.9–1.04)	0.045
DEXA FM (%)	47.57 (7.67)	(43.2–53.5)	44.5 (11.35)	(37.63–53.7)	45.8 (10.04)	(39.65–53.7)	0.042
DEXA FM (kg)	59.04 (17.2)	(45.85–68.2)	49.29 (21.32)	(34.71–61.97)	53.42 (20.21)	(42.07–65.67)	0.002
DEXA FFM (kg)	59.2 (14.38)	(49.03–71.66)	55.67 (12.58)	(46.15–65.7)	57.17 (13.44)	(47.3–66.83)	0.106
HDL cholesterol (mg/dL)	50.18 (20.86)	(38–56.5)	54.69 (17.12)	(43–64.75)	52.88 (18.8)	(40–61)	0.074
LDL cholesterol (mg/dL)	110.6 (36.09)	(84.75–130.25)	112.11 (43.91)	(92–127)	111.51 (40.89)	(91.25–128)	0.766
Total cholesterol (mg/dL)	178.98 (32.31)	(155-201)	186.47 (39.73)	(162.25–207.75)	183.48 (37.06)	(159–202.75)	0.103
Triglycerides (mg/dL)	141.24 (64.54)	(94.25–184.5)	131.73 (69.66)	(87–160)	135.55 (67.68)	(90–168)	0.271
Plasma glucose (mg/dL)	100.54 (26.08)	(85.75–105.25)	98.71 (24.25)	(82–109.75)	99.44 (24.96)	(83–108)	0.576
Plasma insulin (IU/mL)	22.66 (19.2)	(11.5–25.7)	18.04 (12.68)	(9–23.2)	19.89 (15.75)	(9.7–25)	0.036
HOMA-IR	5.84 (5.86)	(2.78–6.44)	4.5 (3.57)	(1.83–5.89)	5.04 (4.66)	(2.07–5.9)	0.043
AST (IU/L)	23.64 (10.31)	(16–29)	22.52 (10.11)	(16–25)	22.97 (10.19)	(16–27)	0.397
ALT (IU/L)	30.2 (20.01)	(16–41)	29.25 (18.11)	(17–36)	29.63 (18.86)	(17–37)	0.704
γGT (IU/L)	37.22 (47.61)	(17–40)	39.45 (54.37)	(19–42)	38.56 (51.68)	(19–40.75)	0.733
Albumin (g/L)	40.55 (2.78)	(39–43)	40.85 (4.21)	(39–42)	40.73 (3.7)	(39–42.75)	0.493
Platelets (10^9/L)	239.19 (53.78)	(199.75–269.25)	232.85 (60.93)	(189.25–266)	235.38 (58.15)	(193.25–266)	0.387
HbA1c (mmol/mol)	40.22 (7.81)	(35–44)	37.04 (12.01)	(26–43)	38.36 (10.57)	(31–44)	0.015
Elastography	5.91 (1.64)	(4.77–6.50)	5.11 (1.94)	(3.42–6.2)	5.43 (1.86)	(4.02–6.30)	0.0005
NAFLD fibrosis score	−0.44 (1.03)	(−1.16–0.26)	−1.01 (1.32)	(−1.99–−0.17)	−0.78 (1.24)	(−1.47–0.08)	<0.001
AST to platelets ratio index	0.24 (0.14)	(0.15–0.29)	0.24 (0.13)	(0.16–0.29)	0.24 (0.13)	(0.15–0.29)	0.692
FIB4	0.96 (0.46)	(0.63–1.12)	0.87 (0.47)	(0.59–1)	0.9 (0.47)	(0.6–1.05)	0.137
	n	**%**	**n**	**%**	**n**	**%**	**P value**
Gender (women)	67	67	84	56	151	60	0.107
Diabetes	35	35	38	25	73	29	0.132
Fibrosis	97	97	100	66.7	197	78.8	<0.001
NASH	61	61	100	67	161	64	0.434
	n	**%**	**n**	**%**	**n**	**%**	**P value**
NAS 0	0	0	21	14	21	8.4	<0.001
NAS 1	24	24	29	19.3	53	21.2	
NAS 2	15	15	0	0	15	6	
NAS 3	16	16	38	25	54	22	
NAS 4	31	31	47	31	78	31	
NAS 5	13	13	13	9	26	10	
NAS 6	0	0	2	1	2	0.80	
NAS 7	1	1	0	0	1	0.40	
SAF-S 0	30	30	50	33	80	32	0.308
SAF-S 1	22	22	41	27	63	25	
SAF-S 2	35	35	49	33	84	34	
SAF-S 3	13	13	10	7	23	9	
SAF-A 0	7	7	50	33	57	23	<0.001
SAF-A 1	25	25	0	0	25	10	
SAF-A 2	61	61	89	59	150	60	
SAF-A 3	7	7	10	7	17	7	
SAF-A 4	0	0	1	0.7	1	0.40	
SAF-F 0	3	3	50	33	53	21	<0.001
SAF-F 1	49	49	46	31	95	38	
SAF-F 2	42	42	43	29	85	34	
SAF-F 3	6	6	11	7	17	7	

BMI, body mass index; DEXA FFM, dual energy X-ray absorptiometry free fat mass; DEXA FM, dual energy X-ray absorptiometry fat mass; HbA1c, haemoglobin A1c; HDL, high-density lipoprotein; HOMA-IR, homeostasis model assessment for insulin resistance; LDL, low-density lipoprotein; NAFLD, non-alcoholic fatty liver disease; NAS, non-alcoholic fatty liver disease activity score; NASH, non-alcoholic steatohepatitis; γGT, γ-glutamyl transferase.

Discovery and validation cohorts

Table 1 reports the characteristics of the patients enrolled in the discovery, validation and global cohorts as well as in the NASH and NAFL groups. Overall, 250 subjects, aged 44.8±11.5 years, of which 60% were women, were studied. While the gender distribution in the two datasets was not different, the subjects in the discovery cohort were older (p=0.014). Diabetes prevalence was 35% in the discovery cohort and 25% in the validation cohort, respectively (p=0.13). The prevalence of hypertension was 56% in the discovery cohort and 60% in the validation cohort (p=0.968), and that of hyperlipidaemia was 45% in the discovery cohort and 49% in the validation cohort (p=0.964). The type and frequency of use of antidiabetic, antihypertensive and antihyperlipidaemic medications are reported in online supplemental table 3.

NASH was not associated with the cohorts: 61% vs 67% (p=0.43). Therefore, we can exclude dataset biases that could potentially affect supervised machine learning, since the primary aim of our study was to identify and validate biomarkers of NASH.

In contrast, the prevalence of liver fibrosis was different in the discovery (97%) and validation cohorts (66.7%) (p<0.001). Therefore, we randomly split the whole database into a discovery and a validation set to obtain a balanced number of patients with and without fibrosis when a model was built to predict fibrosis, but preserving the overall class distribution of the data.

Table 1 shows the two cohorts differed in anthropometric characteristics. While plasma glucose levels did not differ between the two samples, plasma insulin and HOMA-IR showed borderline statistical significance (p=0.036 and p=0.043, respectively). On histological examination, 20% of all participants had liver steatosis<5%, had no inflammation and no ballooning; 15.6% (NAS 3, ie, NAFL) had liver steatosis >5%, did not have or did have inflammation or had liver steatosis >5% did not have or did have ballooning; and 64.4% had NASH (NAS≥3). Liver fibrosis was observed in 78.8% of participants.

The relecture of the histological scores on digitalised images by a second independent pathologist (JC-M) yielded 85% accordance with the centralised lecture (FMV). The results provided derived from the agreement of the two pathologists.

The mean PLIN2 levels in the subjects with NAFL were 1.72±0.40 vs 4.58±1.70 MFI in the group with NASH (p<0.0001, Mann-Whitney U test).

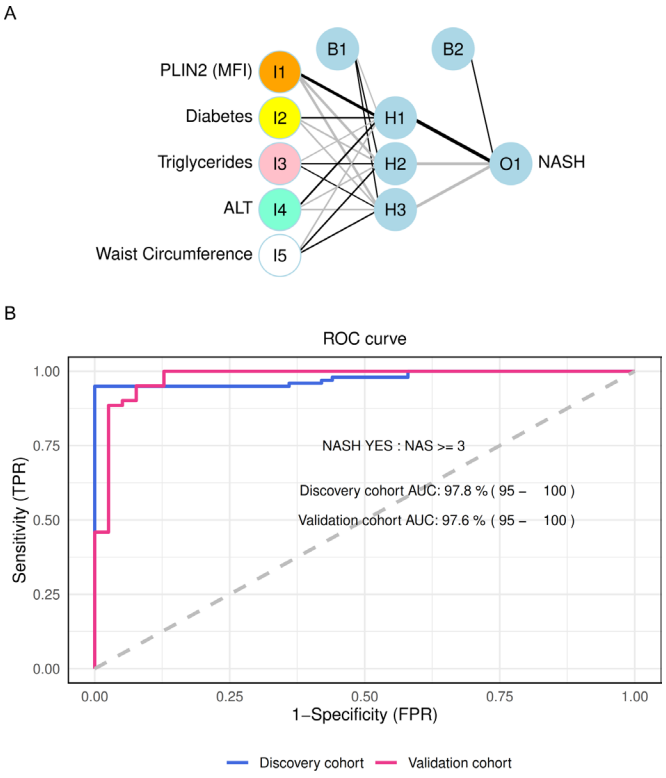

Figure 2 PLIN2 diagnostic performance for predicting presence/absence of NASH. (A) Architecture of the NN used. Each input node represents a biomarker, while edges represent the weights between layers. The thickness of the edge is proportional to the magnitude of each weight.Positive weights are plotted as black lines; negative weights as grey lines. In the NN, there are five input nodes: PLIN2, presence of diabetes, plasma triglycerides and ALT levels and waist circumference. There are three hidden nodes and one output node for presence of NASH. Two biases nodes are included. The bias node covers the same function of the intercept in a regression model. (B) ROC curves for predicting the presence of NASH (NAS ≥3) in the discovery and in the validation cohorts. FPR=1−specificity. AUC, area under the curve; B, bias weight; FPR, false-positive rate; H, hidden node; I, input node; MFI, mean florescence intensity; NAS, Non-alcoholic Fatty Liver Disease Activity Score; NASH, non-alcoholic steatohepatitis; NN, neural network; O, output node; PLIN2, perilipin-2; ROC, receiver operating characteristic; TPR, true-positive rate.

NASH prediction

The NN analysis for the prediction of presence/absence of NASH produced an accuracy of 93% in the discovery and of 92% in the validation cohort; the AUCs were 97.8% (CI 95% to 100%) and 97.6% (CI 95% to 100%), respectively. Sensitivity and specificity were 95% and 90% in the discovery cohort and 88% and 100% in the validation cohort, respectively. All the subjects in the validation cohort without histological NASH were correctly predicted as having a NAS score of <3. Eight per cent of individuals with NASH, who were misclassified as being without NASH, had a NAS score of 3. The Olden algorithm identified PLIN2 in monocytes as the most important variable in classifying subjects with and without NASH, followed by presence of diabetes and ALT levels. Figure 2A shows the NN composition; the AUROC curves for both cohorts are reported in figure 2B.

The model including only PLIN2 in monocytes as predictor produced an accuracy of 93% in the discovery cohort, with a sensitivity and specificity of 98.4% and 84.6%, respectively. Values in the validation cohort were 90%, 85% and 100%, respectively.

We also used an NN analysis (figure 3A) to predict the stages of NASH. Also in this case, the Olden algorithm identified monocyte PLIN2 as the most important variable in classifying subjects according to NAS levels. The classification had an accuracy of 85% in the discovery and 85.2% in the validation cohort. Twenty-one subjects without histologically proven NASH were correctly classified in the NAS level=0 class (ie, NAS score <3). Figure 3B shows the ROC curves for each NAS level in the validation cohort. The AUROC ranges from 83.7% (CI 75.6% to 91.8%) to 97.8% (CI 95.8% to 99.8%). The average levels of PLIN2 in monocytes in the three classes of NAS are depicted in figure 4.

Two Excel files implementing the estimated networks to facilitate NASH diagnosis and NAS level prediction are provided in the online supplemental material.

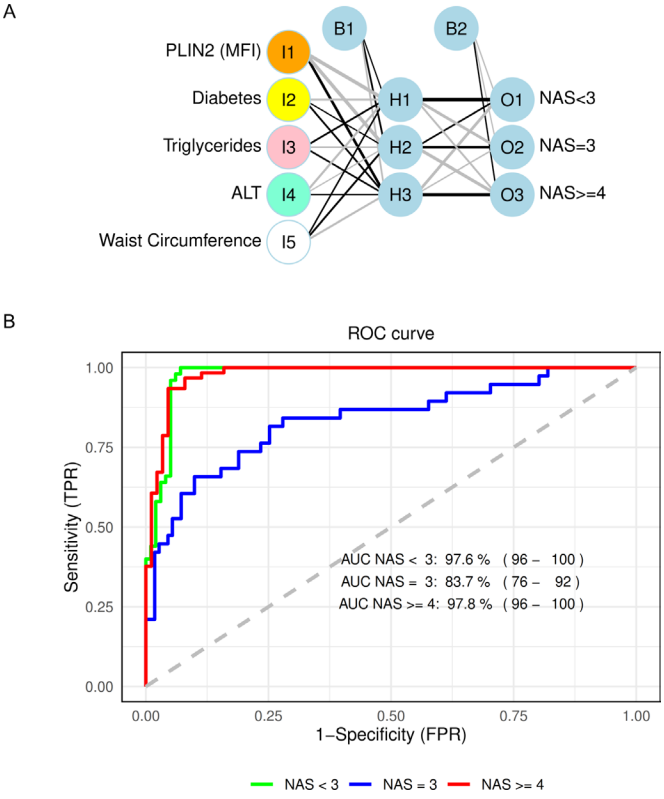

Figure 3 PLIN2 diagnostic performance for predicting NASH severity. (A) PLIN2 biomarker network for diagnosing of NASH severity through NAS levels. Architecture of the NN used. Each input node represents a biomarker, while edges represent the weights between layers. The thickness of the edge is proportional to the magnitude of each weight . Positive weights are plotted as black lines; negative weights as grey lines. In the NN, there are five input nodes: PLIN2, presence of diabetes, plasma triglycerides and ALT levels and waist circumference. There are three hidden nodes and three output nodes for NAS level=0 for total NAS score <3, NAS level=1 for total NAS score=3, NAS level=2 for total NAS score ≥4. Two bias nodes are included. The bias node covers the same function of the intercept in a regression model. (B) ROC curves for each level of NASH severity as identified by the NAS value (see aforementioned) in the validation cohort. FPR=1−specificity. AUC, area under the curve; B, bias weight; FPR, false-positive rate; H, hidden node; I, input node; MFI, mean fluorescence intensity; NAS, Non-alcoholic Fatty Liver Disease Activity Score; NASH, non-alcoholic steatohepatitis; NN, neural network; O, output node; PLIN2, perilipin-2; ROC, receiver operating characteristic; TPR, true-positive rate.

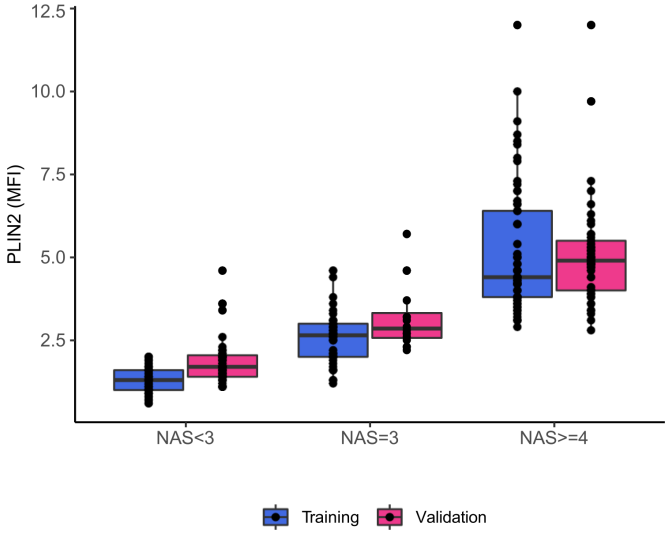

Figure 4 Whisker plots of monocyte PLIN2 levels (MFI) measured by flow cytometry in the training and validation cohorts in different NASH stages: histological NAS <3, NAS=3 and NAS ≥4. MFI, mean fluorescence intensity; NAS, Non-alcoholic Fatty Liver Disease Activity Score; NASH, non-alcoholic steatohepatitis; PLIN2, perilipin-2.

SAF-A prediction

In 2012, Bedossa *et al*[30] described the SAF scoring system, which includes steatosis, activity and fibrosis and was proposed to aid in distinguishing between NAFL and NASH in subjects with morbid obesity.

SAF-A score is the activity part of the SAF scoring system that incorporates scores for ballooning and inflammation. Although NAS continues to be the most used score for the histologic diagnosis of NASH, a decrease of 2 points of SAF-A or more has been adopted as primary endpoint in some RCTs.[39]

Online supplemental figure 2 shows the monocyte levels of PLIN2 at different degrees of NASH severity, according to SAF-A.

Both the Youden and the closest top-left criteria led to a threshold of 0.38, according to which the accuracy of the algorithm was 98.4% in the discovery cohort with a sensitivity of 100% and a specificity of 93%; accuracy, sensitivity and specificity were 96%,100% and 82% when the same threshold was applied to the validation sample. The diagnostic ability of the model is shown in online supplemental figure 3, where the ROC curve is reported along with the identified threshold, AUROC, sensitivity and specificity.

The model predicted SAF-A levels with an accuracy of 89% in the discovery and 84% in the validation samples (online supplemental table 4).

Liver fibrosis prediction

RAB14 was used to predict liver fibrosis with a logistic model including also waist circumference, age, plasma glucose, high-density lipoprotein (HDL) cholesterol and ALT. The predictors were those variables, which were significant in a univariate analysis (online supplemental table 5) and represented a particular physiological aspect, the metabolic, lipidic and hepatic ones. The AUROC with its CI, calculated using bootstrap replicates, was 95.9% (CI: 87.6% to 100%) in the discovery sample. Accuracy, sensitivity and specificity were 99.2%, 100% and 95.8%, respectively, when the Youden criterium was adopted as classification factor with a threshold of 0.55. In the validation sample, AUROC was 99.3% (CI 98.1% to 100%); accuracy was 97.6%; sensitivity was 99% and specificity and 89.6%.

When RAB14 was used as the only variable in the model, accuracy, sensitivity and specificity were 86.4%, 96.0% and 45.8%, respectively, in the discovery cohort. In the validation cohort, they were 82.4%, 96.9% and 34.5%, respectively. In both cohorts, half of subjects without fibrosis were erroneously predicted as being with fibrosis (13/24 and 19/29); however, the diagnosis of fibrosis was correctly predicted (97/101 and 93/96). The use of glycaemia as a covariate increases the specificity to 87.5% and to 86.2% in the discovery and validation cohorts, respectively.

Figure 5 shows the AUROC of the model containing RAB14 (figure 5A) for the prediction of presence/absence of liver fibrosis in the discovery dataset and the RAB14 monocyte levels at SAF-F=0 (presence of fibrosis) and SAF-F ≥1 (figure 5B).

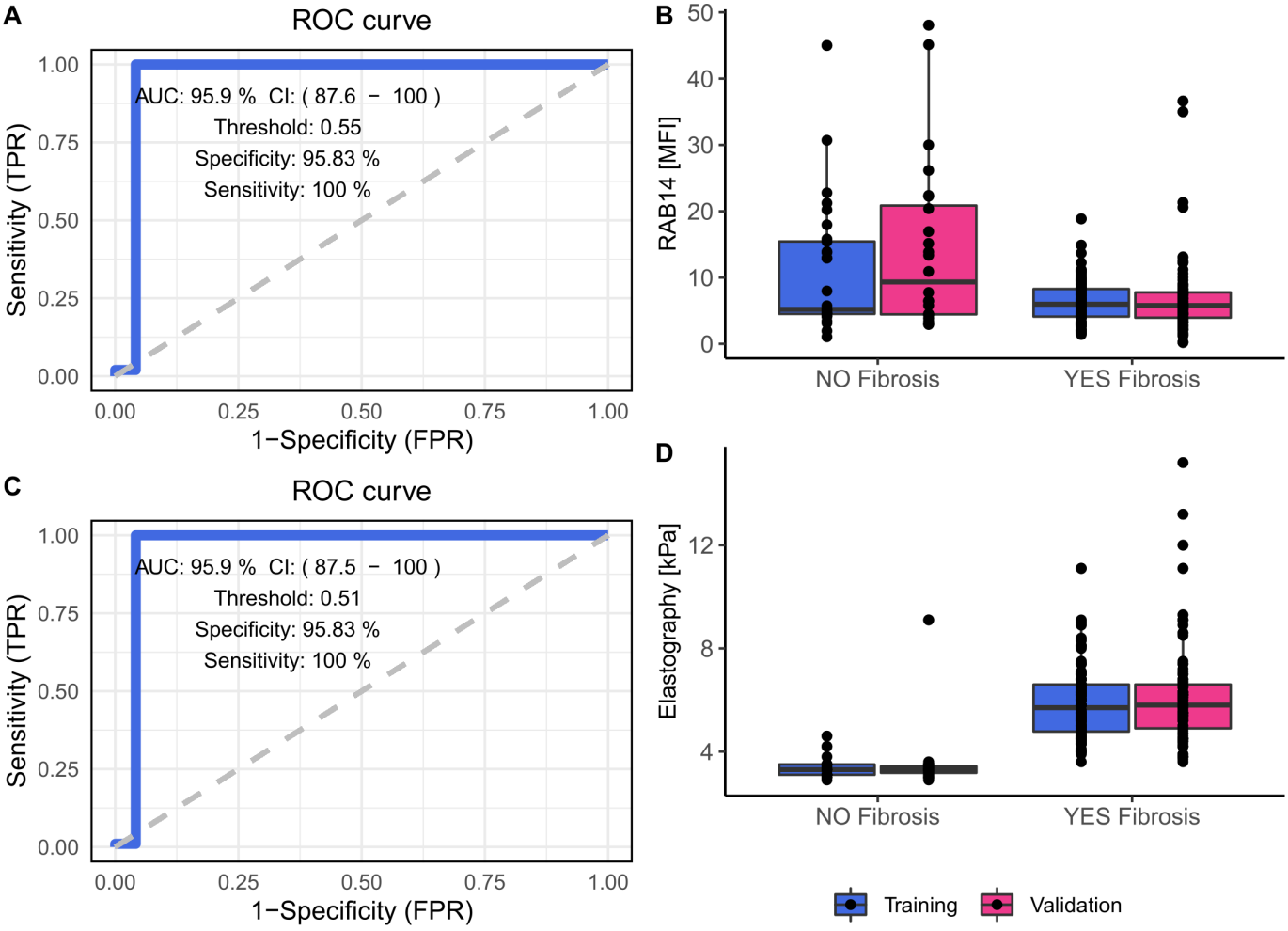

Figure 5 RAB14 (A) and elastography (C) diagnostic performance for presence/absence of NASH. The model estimates ±SE (A) (RAB14) are intercept −62.25±22.15, RAB14 −0.87±0.81, waist circumference 12.03±4.28, plasma glucose 1.09±3.66, age 3.33±2.40, HDL cholesterol −1.80±4.64 and ALT −0.23±1.25. The model estimates ±SE (C) (elastography) are intercept −61.69±22.84, elastography 2.49±2.48, waist circumference 10.1±4.84, plasma glucose 1.64±3.74, age 2.97±2.49, HDL cholesterol −1.43±1.70 and ALT −0.16±1.22. Monocyte RAB14 levels (MFI) measured by flow cytometry at Steatosis, Activity, Fibrosis-Fibrosis (SAF-F) scores 0 (NO Fibrosis), ≥1 (YES Fibrosis) in the training and validation cohorts (B). Ultrasound transient elastography (kPa) at SAF-F scores 0 (NO Fibrosis), ≥1 (YES Fibrosis) in the training and validation cohorts (D). AUC, area under the curve; FPR, false-positive rate; HDL, high-density lipoprotein; MFI, mean fluorescence intensity; ROC, receiver operating characteristic; TPR, true-positive rate.

The model accuracy in predicting fibrosis severity (SAF-F levels) was 69.6% in both the discovery and validation samples.

If the fibrosis stage was recoded as a three-level variable assuming values of 0 if SAF-F ≤1, 1 if SAF-F=2 and 2 if SAF-F=3, then the two models, one including RAB14 and other including elastography, produced the following accuracies: 67.2% and 63.2% in the discovery and validation cohorts, respectively, for RAB14, and 65.6% in both the discovery and validation cohort for elastography. For the model including RAB14, the greatest percentage of misclassified individuals was those with SAF-F=2 who were classified in the lower level (SAF-F ≤1). The same occurred for elastography.

Elastography

When RAB14 was replaced with the variable of elastography liver stiffness in the same algorithm to predict presence/absence of fibrosis, AUROC was 95.9% (CI 87.5% to 100%), accuracy=98.4%, sensitivity=99.01% and specificity=95.8% in the discovery dataset. AUROC=99.2% (CI 98% to 100%), accuracy=96%, sensitivity=98% and specificity=91.5% were demonstrated in the validation dataset when the same Youden threshold of 0.51 was used.

No differences were found between the two models in terms of AUROCs in either the discovery or the validation datasets (p=0.48 and p=0.34, respectively).

Figure 5 shows the AUROC of the model containing elastography (kPa) (figure 5C) for the prediction of presence/absence of liver fibrosis in the discovery dataset and the RAB14 monocyte levels at SAF-F=0 and SAF-F ≥1 (figure 5D).

When the elastography variable was used instead of RAB14 in the multinomial model predicting SAF-F level, the accuracy was 68% in the discovery sample and 68.8% in the validation sample. RAB14 performance in diagnosing the severity of liver fibrosis was comparable to that of elastography.

RAB14 versus FIB4, AST-to-platelet ratio and NAFLD fibrosis score

The RAB14 algorithm was compared with the predictive capacity of FIB4, NAFLD fibrosis score and AST-to-platelet ratio index

to diagnose liver fibrosis in the validation cohort. The highest AUROC value was obtained with the new algorithm (99.3%, CI 98.1% to 100%), which was significantly higher than the AUROCs obtained with the other indices: AUROC NAFLD fibrosis score=85.2% (CI 77% to 92.3%) (p=0.0002), AUROC FIB4=62.2% (CI 49.8% to 74.6%) (p<0.0001) and AUROC AST-to-platelet ratio=61.8% (CI 51.3% to 72.6%) (p<0.0001).

Online supplemental figure 4 reports the ROC curves for each of the aforementioned indices.

Therefore, the algorithm containing RAB14 outperformed currently used biomarkers of liver fibrosis.

NASH and liver fibrosis prediction in subjects with diabetes and/or obesity

We wanted to verify how well the new biomarkers predicted NASH and fibrosis in subjects with diabetes and/or obesity. To this end, we used two stepwise regression models, one testing the dependence of PLIN2 on BMI, presence or absence of NASH, and presence or absence of diabetes. We also tested the dependence of RAB14 on BMI, presence or absence of liver fibrosis, and presence or absence of diabetes. NASH (β=2.27, p<0.0001) and BMI (β=0.04, p=0.006) were the only predictors of PLIN2. A further model including all the variables used to predict NASH was tested in a stepwise regression procedure. The variables entered the model were therefore, in addition to BMI and diabetes, triglycerides, ALT and waist circumference. The only significant predictors in the final model were NASH (β=1.80, p<0.0001), BMI (β=0.037, p=0.005), triglycerides (β=0.003, p<0.046) and ALT (β=0.025, p<0.0001).

When only BMI and diabetes were considered as predictors of RAB14, it depended only on the presence of liver fibrosis (β=−5.66, p<0.0001), while BMI and diabetes were not significant predictors and were excluded from the final model by the stepwise selection procedure. When also age, ALT, HDL, waist circumference and plasma glucose were tested into the model, the only predictors of RAB14 were age (β=0.13, p<0.0001) and fibrosis (β=−7.64, p<0.0001).

Patients were then divided into two BMI classes, subjects without or with class 2 obesity, BMI of <35 and BMI of ≥35. The performance of the two algorithms, the one including PLIN2 and the other one including RAB14, were evaluated in terms of accuracy. PLIN2 had an accuracy of 81% for predicting NAS level in the subgroup of 178 subjects with severe obesity and an accuracy of 87.7% in the subgroup of 73 patients suffering from diabetes. Sixty-six subjects had both obesity and diabetes; in this subgroup, the accuracy of our algorithm was 87.9% (online supplemental figure 5). In the subgroup of subjects with BMI of <35, the accuracy was 95.8%.

When the algorithm with RAB14 was used, its accuracy in predicting liver fibrosis (presence/absence) was 95.8% in the subgroup of subjects with obesity, 100% in the subgroup with diabetes, and 100% in the subgroup of patients with both obesity and diabetes.

Accuracies were 62%, 68.5% and 68.2% when predicting fibrosis stages, respectively.

Patients were then divided into two BMI classes, subjects without or with obesity, BMI of <30 and BMI of ≥30, and the performance of the two new algorithms was evaluated in terms of accuracy (online supplemental figure 5). The algorithm with PLIN2 predicted the NAS levels with an accuracy of 81.2% in the subgroup of 196 subjects with obesity and with an accuracy of 87.7% in 73 patients with diabetes. All patients with diabetes had a BMI of ≥30; therefore, the accuracy was the same than in those patients with obesity. Accuracy in the subsample of 53 patients with BMI of <30 was 100%. The accuracy of the algorithm with RAB14 in predicting SAF-F levels was 62.9% in patients with obesity and 68.5% in those with diabetes. Using liver stiffness elastography variable instead of RAB14 allowed an accuracy of 61% and 63% in patients with obesity and/or diabetes, respectively. The misclassified patients with obesity were mostly subjects with SAF-F equal to 1 but who were predicted as having a more severe condition (SAF-F_level=2) or vice versa their fibrosis severity was underestimated, they were predicted in the SAF-F_level=1 class when instead had an SAF-F ≥2 (in total 35% for RAB14 and 37.6% for elastography).

NASH and fibrosis prediction before and after metabolic surgery

Fifty patients with histologically proven NASH who underwent RYGB were included in this study (BRAVES RCT). Ultrasound-guided needle liver biopsy was performed at 1 year after surgery. The patients lost an average of 37 kg corresponding to 28.8% wt loss. Anthropometry, plasma glucose and insulin, HOMA-IR, lipid profile, blood pressure and liver enzymes levels are reported in table 2; all variables were significantly improved after metabolic surgery. NASH was fully reversed in 74% of participants according to the values of NAS; however, while the severity of liver fibrosis improved, the fibrosis did not disappear. Actually, the prevalence of SAF-F1 increased from 46% to 70%, while that of SAF-F2 halved from 46% to 22%, and SAF-F3 decreased from 8% to only 2%.

We evaluated the performance of the two new algorithms in this external cohort.

The accuracies were 75.5% and 87.5% before and after surgery, respectively, for NAS level prediction. The accuracy in predicting SAF-F levels before surgery was 67.3%. Since bariatric surgery causes changes in metabolism and has effects on several mechanisms, the model developed on a population with 78.8% of individuals with moderate to severe obesity could be inappropriate to predict a population of an individuals who underwent metabolic surgery. The model, including the same variables, was therefore fitted on the surgery population, and the accuracy was 81.2% for SAF-F level prediction using RAB14. Online supplemental table 6 reports the coefficients of the model for the surgery cohort. When the TE variable was used in place of RAB14, accuracy was 73.5%. No significant differences were observed between the predictivity of RAB14 and elastography algorithms.

Data in the group of subjects who underwent metabolic surgery are graphed in online supplemental figure 6.

DISCUSSION

We show that a liquid biopsy using circulating monocytes can accurately predict the presence and severity of NASH as well as liver fibrosis in subjects without other causes of chronic liver disease or steatosis.

An algorithm containing PLIN2, as measured in peripheral blood monocytes, had an accuracy between 92% and 93%, sensitivity of 88%–95% and specificity of 90%–100% for the diagnosis of NASH. Similarly, an algorithm with RAB14 in circulating monocytes had an accuracy between 99.2% and 97.6%, sensitivity of 90%–98% and specificity of 87%–93% for the diagnosis of liver fibrosis. Unlike other algorithms in the literature,[11–18] ours was able to discriminate among various stages of NASH severity.

Table 2 Characteristics of the subjects in the metabolic surgery cohort, baseline and 1-year postsurgery data

	Before RYGB 50 subjects		After RYGB 50 subjects		
Variable name	**Mean (SD)**	**(1st–3rd IQR)**	**Mean (SD)**	**(1st–3rd IQR)**	**P value**
Age	48.72 (8.94)	(44–54)	49.72 (8.94)	(45–55)	–
Weight (kg)	128.52 (25.47)	(108.75–149.25)	91.52 (25.1)	(75–103)	<0.0001
Height (cm)	171.14 (9.96)	(162–179.75)	171.14 (9.96)	(162–179.75)	–
BMI (kg/m^2)	43.4 (5.51)	(39–47.6)	31.18 (7.22)	(26.68–33.95)	<0.0001
Hip circumference (cm)	131.18 (14.6)	(122–140)	110.35 (14.43)	(101–116)	<0.0001
Waist circumference (cm)	132.12 (18.2)	(120–148)	103.57 (19.07)	(94–115)	<0.0001
Waist to hip ratio	1 (0.1)	(0.9–1.1)	0.94 (0.11)	(0.9–1)	<0.0001
DEXA FM (%)	49.37 (4.44)	(46.48–51.43)	33.35 (8.12)	(27.1–38.85)	<0.0001
DEXA FM (kg)	60.53 (13.27)	(51.70 - 71.17)	29.48 (12.33)		<0.0001
DEXA FFM (kg)	62.58 (11.99)	(50.48–73.5)	56.11 (12.44)	(45.18–67.25)	<0.0001
HDL cholesterol (mg/dL)	46.98 (16.25)	(37–50)	51.96 (15.68)	(41.25–60.75)	0.089
LDL cholesterol (mg/dL)	113.28 (32.53)	(95.25–130.75)	95.26 (37.04)	(71.5–108)	0.001
Total cholesterol (mg/dL)	189.25 (29.72)	(162.75–206.75)	163.42 (36.81)	(138.5–188.25)	<0.0001
Triglycerides (mg/dL)	153.16 (72.77)	(109–184)	90.06 (51.17)	(60–108)	<0.0001
Plasma glucose (mg/dL)	116.18 (37.62)	(96–125.25)	82.06 (15.58)	(74–86)	<0.0001
Plasma insulin (IU/mL)	30.1 (16.9)	(17–42)	10.32 (6.57)	(7–11.75)	<0.0001
HOMA-IR	9.2 (6.93)	(3.68–11.6)	2.16 (1.61)	(1.25–2.5)	<0.0001
AST (IU/L)	31.24 (17.48)	(20–40.75)	23.02 (11.98)	(16–27)	0.009
ALT (IU/L)	42.46 (27.72)	(21.25–51.25)	25.7 (23.42)	(14–32.25)	0.002
γGT (IU/L)	51.15 (86.34)	(23.75–45.25)	22.65 (23.66)	(12–23)	0.004
Albumin (g/L)	41.08 (2.97)	(39–43)	41.21 (3.14)	(38.75–43.25)	0.863
Platelets (10^9/L)	222.76 (52.87)	(192 - 250)	202.71 (55.01)	(166 - 226)	0.001
HbA1c (mmol/mol)	44.17 (10.96)	(37 - 47)	36.94 (5.86)	(34–38)	<0.0001
PLIN2 MFI	4.4 (1.53)	(3.2–5.5)	1.93 (0.75)	(1.43–2.21)	<0.0001
RAB14 MFI	7.02 (2.3)	(5.45–8.28)	14.08 (4.85)	(9.85–17.38)	<0.0001
Elastography (kPa)	6.09 (1.47)	(5.33–6.6)	5.04 (1.05)	(4.5–5.58)	<0.0001
NAFLD fibrosis score	0.28 (1.1)	(–0.47–0.91)	–0.98 (1.26)	(–1.83––0.19)	<0.0001
AST to platelets ratio index	0.24 (0.05)	(0.2–0.26)	0.24 (0.05)	(0.21–0.27)	<0.0001
FIB4	1.15 (0.6)	(0.66–1.57)	1.25 (0.47)	(0.87–1.58)	0.169
	n	**%**	**n**	**%**	**P value**
Gender (women)	22	44	–	–	
Diabetes	27	54	8	16	0.0002
Fibrosis	50	100	47	94	0.240
NASH	50	100	13	26	<0.0001
	n	**%**	**n**	**%**	**P value**
NAS 0	0	0	37	74	<0.0001
NAS 3	15	30	10	20	
NAS 4	21	42	2	4	
NAS 5	13	26	1	2	
NAS 6	1	2	0	0	
NAS 7	0	0	0	0	
SAF-S 0	0	0	35	70	<0.001
SAF-S 1	15	30	9	18	
SAF-S 2	27	54	6	12	
SAF-S 3	8	16	0	0	
SAF-A 0	0	0	1	2	<0.001
SAF-A 1	1	2	26	52	
SAF-A 2	39	78	22	44	
SAF-A 3	10	20	1	2	
SAF-A 4	0	0	0	0	
SAF-F 0	0	0	3	6	0.005
SAF-F 1	23	46	35	70	
SAF-F 2	23	46	11	22	
SAF-F 3	4	8	1	2	

BMI, body mass index; DEXA FFM, Dual Energy X-Ray Absorptiometry Free Fat Mass; DEXA FM, Dual Energy X-Ray Absorptiometry Fat Mass; HbA1c, Haemoglobin A1c; HDL, high-density lipoprotein; HOMA-IR, Homeostasis Model Assessment of Insulin Resistance; LDL, low-density lipoprotein; MFI, mean fluorescence intensity; NAFLD, non-alcoholic fatty liver disease; NAS, Non-alcoholic Fatty Liver Disease Activity Score; NASH, non-alcoholic steatohepatitis; PLIN2, perilipin-2; RYGB, Roux-en-Y gastric bypass; γGT, γ-Glutamyl Transferase.

The algorithm with RAB14 outperformed currently used biomarkers of liver fibrosis, such as FIB4, NAFLD fibrosis score or AST-to-platelet ratio, and gave results comparable to those of elastography. Both PLIN2 and RAB14 algorithms diagnosed with accuracy a significant liver fibrosis (≥F2) in association with NASH severity (NAS ≥4), a rapidly worsening condition which represents the target for therapeutical RCTs. Finally, the new algorithms well predicted histological improvement of NASH and liver fibrosis after metabolic surgery, and thus they can be used not only as diagnostic but also as monitoring biomarkers. However, although the severity of liver fibrosis declined after metabolic surgery, the prevalence of SAF-F1 increased from 46% to 70%. This can explain why our algorithm including RAB14 as well as that with elastography had a reduced performance.

Our algorithm for NASH diagnosis and staging did not include BMI in order to avoid introducing a bias inherent to body weight. In fact, NASH is present also in subjects with normal weight as shown, for instance, in the GOASIA registry where the prevalence of NAFLD in subjects with a BMI <25 kg/m^2 ranged from 7.6% to 25.6% and a substantial proportion of these subjects (50.5%) had biopsy-proven NASH.[40] In a meta-analysis, 39% of subjects with NAFLD and normal weight or overweight had NASH; 29.2% had stage ≥2 liver fibrosis; and 3.2% had cirrhosis.[41]

Indeed, our algorithm showed a good sensitivity and specificity also in the validation cohort where the BMI was lower compared with the discovery cohort, with a range of 23.1–42.43 kg/m^2 vs 38.53–46.03 kg/m^2.

We used the presence/absence of diabetes as a covariate in the NN analysis because of the high prevalence of NASH among patients with T2D. In fact, in a meta-analysis, the estimated prevalence of NASH among individuals with T2D was 37.3% (95% CI 24.7% to 50.0%) and that of advanced liver fibrosis 17.0% (95% CI 7.2 to 34.8).[42]

Fibrosis is often associated with NASH and has important implications for clinical outcomes; therefore, an effective treatment for NASH must, at least, prevent liver fibrosis progression.

In our study, the performance of RAB14 algorithm in diagnosing liver fibrosis presence and stages was comparable with that of ultrasound two-dimensional shear wave elastography.

Liver stiffness evaluated with elastographic techniques is expensive, operator-dependent and machine-dependent, and may be not feasible in patients with severe obesity when the skin–liver capsule distance is higher than 5 cm or in patients with thin intercostal spaces.[43]

Measuring PLIN2 and RAB14 in monocytes is inexpensive and scalable with up to 800 samples that can be analysed in a single day. Usually, immunophenotyping is performed in fresh blood or in polymorphonuclear cells the same day or within 24 hours of collection. We demonstrated that cryopreserved is comparable to fresh blood for monocyte flow-cytometry studies making possible to postpone and centralise analyses.

PLIN2 and RAB14 may permit diagnosis of NASH and/or liver fibrosis with a simple blood test. Our biomarkers can be used in community and population studies permitting to investigate the real prevalence of NASH and liver fibrosis. Moreover, since it requires only blood sampling, they are potentially valuable tools for population-based and prevention studies in children.

Strengths of our multicentre study include that liver histology was available in all subjects. A limitation is that only Caucasian subjects were enrolled, thus limiting the generalisability of our results to other ethnicities, although no differences between ethnicities are expected. Another limitation of our study is the different prevalence of liver fibrosis in the discovery (97%) and validation (67%) cohorts (p<0.001). To cope with this, we randomly split the whole database into a discovery and a validation set to obtain a balanced number of patients with and without fibrosis when a model was built to predict fibrosis while preserving the overall class distribution of the data.

In conclusion, new liquid biopsy tests that use peripheral blood monocyte PLIN2 and RAB14 as biomarkers were reliable in diagnosing NASH and/or liver fibrosis. PLIN2 and RAB14 have the potential to replace invasive liver biopsy-based histology for the diagnosis and management of NASH and liver fibrosis.

Due to the epidemic nature of metabolic liver diseases, rapid and cost-effectiveness tests for the diagnosis of NASH and liver fibrosis can permit the study of their prevalence in the general population and to monitor the effects of lifestyle, surgical and pharmacological interventions.

Author affiliations
[1]Università Cattolica del Sacro Cuore, Rome, Italy
[2]Department of Medical and Surgical Sciences, Fondazione Policlinico Universitario A. Gemelli IRCCS, Rome, Italy
[3]CNR-IASI,Consiglio Nazionale delle Ricerche, Istituto di Analisi dei Sistemi ed Informatica, Laboratorio di Biomatematica, Rome, Italy
[4]Department of Surgical Sciences, University of Rome La Sapienza, Rome, Italy
[5]Department of Pathology and Laboratory Medicine, Fondazione Policlinico Universitario A. Gemelli IRCCS, Rome, Italy
[6]San Camillo Forlanini Foundation, Roma, Italy
[7]Bariatric and Metabolic Surgery; King's College Hospital, London, UK
[8]Diabetes Complications Research Centre, Conway Institute, University College Dublin, Dublin, Ireland
[9]Department of Medicine III, Universitätsklinikum Carl Gustav Carus an der Technischen Universität Dresden, Dresden, Germany
[10]Division of Diabetes & Nutritional Sciences, School of Cardiovascular and Metabolic Medicine & Sciences, King's College London, London, UK

Acknowledgements We would like to thank Mrs. Anna Caprodossi, an invaluable technician.

Contributors GM, GA, SP, CWIR, SRB and FR designed the study. SP and FP did the statistics. GA did the analyses. LC-G, GC, MR, LC, PLM, OV, MG, JRC-M and MFR carried out the study. MP, LR and MG performed the liver biopsies and hepatological follow-up. FMV, pathologist, read all liver biopsies. JRC-M reread the biopsies. GM, GA, SP, LC-G, CWIR, SRB and FR wrote the first draft. GM and SP are guarantors of the data. All authors actively contributed to the definitive version.

Funding Microbesomics: effect of gut microbiome on 'obesitypes' in human subjects (PRIN 2017 n. 2017FM74HK_004), Elucidating Pathways of Steatohepatitis (EPoS) (EPOS Horizon 2020 n. MIN-EPO-17-013), Stratification of Obese Phenotypes to Optimize Future Obesity Therapy (SOPHIA IMI n. 875534). Metadeq Inc. GM and SB acknowledge support from the Transcampus Initiative.

Competing interests GM reports consulting fees from Novo Nordisk,_Fractyl Inc and Recor Inc; she is also scientific current advisor and consultant of Metadeq Limited, and current advisor and consultant of Keyron Limited, GHP Scientific Limited, and Jemyll Limited. FR reports receiving research grants from Ethicon and Medtronic; consulting fees from Novo Nordisk, Ethicon and Medtronic; serving on scientific advisory boards for GI Dynamics; and is former director and current stock option holder of Metadeq Limited and former director and current advisor of Keyron Limited and GHP Scientific Limited. CWIR reports grants from the Irish Research Council, Science Foundation Ireland, Anabio and the Health Research Board; serves on advisory boards of Novo Nordisk, Herbalife, GI Dynamics, Eli Lilly, Johnson & Johnson, Sanofi Aventis, AstraZeneca, Janssen, Bristol-Myers Squibb, Glia and Boehringer Ingelheim. CIR is a member of the Irish Society for Nutrition and Metabolism outside the area of work commented on here, and is the chief medical officer and director of the Medical Device Division of Keyron since January 2011; both of these are unremunerated positions. CWIR is also current director, shareholder and stock option holder of Metadeq Limited, current director of GHP Scientific Limited, was a previous investor in Keyron, which develops endoscopically implantable medical devices intended to mimic the surgical procedures of sleeve gastrectomy and gastric bypass. The product has only been tested in rodents and none of Keyron's products are currently licensed. They do not have any contracts with other companies to put their products into clinical practice. No patients have been included in any of Keyron's studies and they are not listed on the stock market. He continues to provide scientific advice to Keyron for no remuneration. All other authors declare no competing interests.

Patient and public involvement Patients and/or the public were not involved in the design, conduct, reporting or dissemination plans of this research.

Patient consent for publication Not applicable.

Ethics approval This study involves human participants and was approved by Fondazione Policlinico Universitario A. Gemelli IRCCS, Rome, Italy (ID 2162). The study protocols were approved by the ethical committees of the Università Cattolica del Sacro Cuore, Università La Sapienza and San Camillo Hospital, all in Rome, Italy. All participants provided written informed consent at the time of enrolment and a further written consent before metabolic surgery.

Provenance and peer review Not commissioned; externally peer reviewed.

Data availability statement All data relevant to the study are included in the article or uploaded as supplementary information.

ORCID iD

Geltrude Mingrone http://orcid.org/0000-0003-2021-528X

REFERENCES

1 Wong VW-S, Chitturi S, Wong GL-H, *et al*. Pathogenesis and novel treatment options for non-alcoholic steatohepatitis. *Lancet Gastroenterol Hepatol* 2016;1:56–67.
2 Pioglitazone vs vitamin E vs placebo for treatment of non-diabetic patients with nonalcoholic steatohepatitis (PIVENS). Available: https:// clinicaltrials.gov/ct2/show/NCT00063622
3 Friedman SL, Ratziu V, Harrison SA, *et al*. A randomized, placebo-controlled trial of cenicriviroc for treatment of nonalcoholic steatohepatitis with fibrosis. *Hepatology* 2018;67:1754–67.
4 Haukeland JW, Damås JK, Konopski Z, *et al*. Systemic inflammation in nonalcoholic fatty liver disease is characterized by elevated levels of CCL2. *J Hepatol* 2006;44:1167–74.
5 Smits MM, van Geenen EJM. The clinical significance of pancreatic steatosis. *Nat Rev Gastroenterol Hepatol* 2011;8:169–77.
6 Guijas C, Meana C, Astudillo AM. Foamy monocytes are enriched in cis-7-Hexadecenoic fatty acid (16:1n-9), a possible biomarker for early detection of cardiovascular disease. *Cell Chem Biol* 2016;2368:9–99.
7 Sztalryd C, Brasaemle DL. The perilipin family of lipid droplet proteins: Gatekeepers of intracellular lipolysis. *Biochim Biophys Acta Mol Cell Biol Lipids* 2017;1862:1221–32.
8 Diehl AM, Day C, Cause DC. Cause, pathogenesis, and treatment of nonalcoholic steatohepatitis. *N Engl J Med* 2017;377:2063–72.
9 Angulo P, Kleiner DE, Dam-Larsen S, *et al*. Liver fibrosis, but no other histologic features, is associated with long-term outcomes of patients with nonalcoholic fatty liver disease. *Gastroenterology* 2015;149:389–97.
10 Karlmark KR, Wasmuth HE, Trautwein C, *et al*. Chemokine-directedimmune cell infiltration in acute and chronic liver disease. *Expert Rev Gastroenterol Hepatol* 2008;2:233–42.
11 Kwok R, Tse Y-K, Wong GL-H, *et al*. Systematic review with metaanalysis: non-invasive assessment of non-alcoholic fatty liver disease--the role of transient elastography and plasma cytokeratin-18 fragments. *Aliment Pharmacol Ther* 2014;39:254–69.
12 Feldstein AE, Lopez R, Tamimi TA-R, *et al*. Mass spectrometric profiling of oxidized lipid products in human nonalcoholic fatty liver disease and nonalcoholic steatohepatitis. *J Lipid Res* 2010;51:3046–54.
13 He L, Deng L, Zhang Q, *et al*. Diagnostic value of CK-18, FGF-21, and related biomarker panel in nonalcoholic fatty liver disease: a systematic review and meta-analysis. *Biomed Res Int* 2017;2017:1–12.
14 Vilar-Gomez E, Chalasani N. Non-invasive assessment of non-alcoholic fatty liver disease: clinical prediction rules and blood-based biomarkers. *J Hepatol* 2018;68:305–15.
15 Cabré N, Luciano-Mateo F, Baiges-Gayà G, *et al*. Plasma metabolic alterations in patients with severe obesity and non-alcoholic steatohepatitis. *Aliment Pharmacol Ther* 2020;51:374–87.
16 Bril F, Millán L, Kalavalapalli S, *et al*. Use of a metabolomic approach to non-invasively diagnose non-alcoholic fatty liver disease in patients with type 2 diabetes mellitus. *Diabetes Obes Metab* 2018;20:1702–9.
17 Mayo R, Crespo J, Martínez-Arranz I, *et al*. Metabolomic-based noninvasive serum test to diagnose nonalcoholic steatohepatitis: results from discovery and validation cohorts. *Hepatol Commun* 2018;2:807–20.
18 Qadri S, Ahlholm N, Lønsmann I, *et al*. Obesity modifies the performance of fibrosis biomarkers in nonalcoholic fatty liver disease. *J Clin Endocrinol Metab* 2022;107:e2008–20.
19 Angelini G, Salinari S, Bertuzzi A, *et al*. Metabolic surgery improves insulin resistance through the reduction of gut-secreted heat shock proteins. *Commun Biol* 2018;1:69.
20 Angelini G, Castagneto Gissey L, Corpo GD, *et al*. Publisher correction: new insight into the mechanisms of ectopic fat deposition improvement after bariatric surgery. *Sci Rep* 2020;10:2786.
21 Wang T, Ma C. The hepatic macrophage pool in NASH. *Cell Mol Immunol* 2021;18:2059–60.
22 Davies LC, Jenkins SJ, Allen JE, *et al*. Tissue-resident macrophages. *Nat Immunol* 2013;14:986–95.
23 Klein I, Cornejo JC, Polakos NK, *et al*. Kupffer cell heterogeneity: functional properties of bone marrow derived and sessile hepatic macrophages. *Blood* 2007;110:4077–85.
24 Hinz B, Phan SH, Thannickal VJ, *et al*. Recent developments in myofibroblast biology: paradigms for connective tissue remodeling. *Am J Pathol* 2012;180:1340–55.
25 Itoh Y. Membrane-type matrix metalloproteinases: their functions and regulations. *Matrix Biol* 2015;44-46:207–23.
26 Jin H, Tang Y, Yang L, *et al*. Rab GTPases: central coordinators of membrane trafficking in cancer. *Front. Cell Dev. Biol.* 2021;9:648384.
27 Bedossa P. Diagnosis of non-alcoholic fatty liver disease/non-alcoholic steatohepatitis: why liver biopsy is essential. *Liver Int* 2018;38 Suppl 1:64–6.
28 Bedossa P, Poynard T. An algorithm for the grading of activity in chronic hepatitis C. the METAVIR cooperative Study Group. *Hepatology* 1996;24:289–93.
29 Kleiner DE, Brunt EM, Van Natta M. Nonalcoholic steatohepatitis clinical research network. design and validation of a histological scoring system for nonalcoholic fatty liver disease. *Hepatology* 2005;41:1313–21.
30 Bedossa P, Poitou C, Veyrie N, *et al*. Histopathological algorithm and scoring system for evaluation of liver lesions in morbidly obese patients. *Hepatology* 2012;56:1751–9.
31 Brunt EM, Kleiner DE, Wilson LA, *et al*. Nonalcoholic fatty liver disease (NAFLD) activity score and the histopathologic diagnosis in NAFLD: distinct clinicopathologic meanings. *Hepatology* 2011;53:810–20.
32 Garcovich M, Faccia M, Di Stasio E, *et al*. Correlation between QElaXto techniques and supersonic Imagine for liver stiffness quantification in chronic liver disease. *J Ultrasound Med* 2022;41:877–86.
33 Goksuluk D, Korkmaz S, Zararsiz G, *et al*. easyROC: an interactive web-tool for ROC curve analysis using R language environment. *R J* 2016;8:213–30.
34 Olden JD, Joy MK, Death RG. An accurate comparison of methods for quantifying variable importance in artificial neural networks using simulated data. *Ecol Modell* 2004;178:389–97.
35 Perkins NJ, Schisterman EF. The inconsistency of "optimal" cutpoints obtained using two criteria based on the receiver operating characteristic curve. *Am J Epidemiol* 2006;163:670–5.
36 DeLong ER, DeLong DM, Clarke-Pearson DL. Comparing the areas under two or more correlated receiver operating characteristic curves: a nonparametric approach. *Biometrics* 1988;44:837–45.
37 R Core Team. R: a language and environment for statistical computing. R foundation for statistical computing, Vienna, Austria, 2013. Available: http://www.R-project.org/
38 Najt CP, Senthivinayagam S, Aljazi MB, *et al*. Liver-specific loss of perilipin 2 alleviates diet-induced hepatic steatosis, inflammation, and fibrosis. *Am J Physiol Gastrointest Liver Physiol* 2016;310:G726–38.
39 Francque SM, Bedossa P, Ratziu V, *et al*. A randomized, controlled trial of the pan-PPAR agonist Lanifibranor in NASH. *N Engl J Med* 2021;385:1547–58.
40 Tan EX-X, Lee JW-J, Jumat NH, *et al*. Non-obese non-alcoholic fatty liver disease (NAFLD) in Asia: an international registry study. *Metabolism* 2022;126:154911.
41 Ye Q, Zou B, Yeo YH, *et al*. Global prevalence, incidence, and outcomes of non-obese or lean non-alcoholic fatty liver disease: a systematic review and meta-analysis. *Lancet Gastroenterol Hepatol* 2020;5:739–52.
42 Younossi ZM, Golabi P, de Avila L, *et al*. The global epidemiology of NAFLD and NASH in patients with type 2 diabetes: a systematic review and meta-analysis. *J Hepatol* 2019;71:793–801.
43 Vuppalanchi R, Siddiqui MS, Van Natta ML, *et al*. Performance characteristics of vibration-controlled transient elastography for evaluation of nonalcoholic fatty liver disease. *Hepatology* 2018;67:134–44.

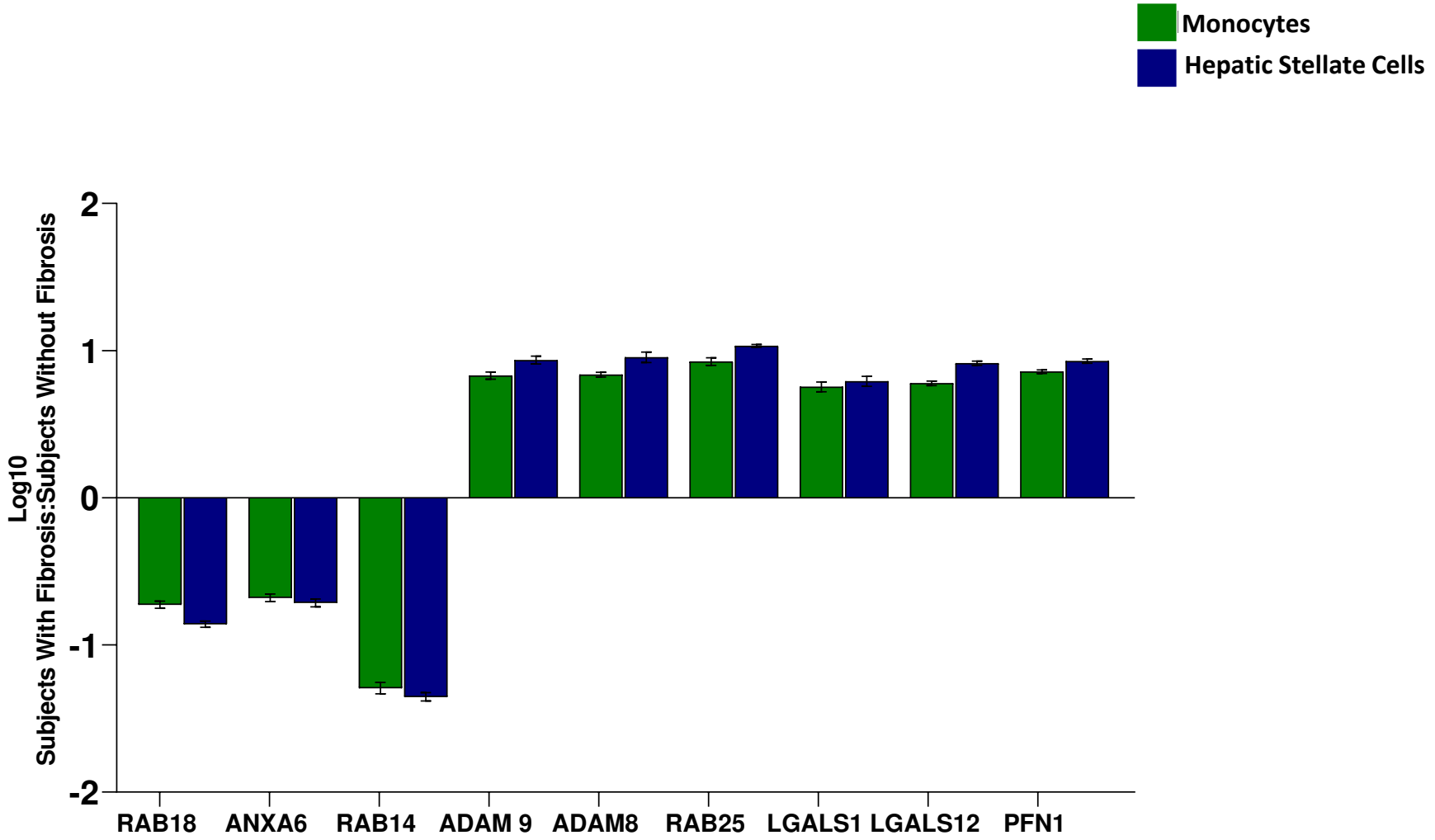
Monocytes
Hepatic Stellate Cells
Log10
Subjects With Fibrosis:Subjects Without Fibrosis
2
1
0
-1
-2
RAB18
ANXA6
RAB14
ADAM 9
ADAM8
RAB25
LGALS1
LGALS12
PFN1

Supplemental Figure 1

iTraQ based analysis of proteins (N=9) differentially expressed in monocytes and hepatic stellate cells (HSCs) of subjects with or without liver fibrosis. Downregulated proteins (N=3) are colored in green while upregulated proteins (N=6) are colored in red.

Ras-related protein Rab-18 (RAB18), Annexin A6 (ANXA6), Ras-related protein Rab-14 (RAB14), Disintegrin and metalloproteinase domain-containing protein 8 and 9 (ADAM 8 and 9), Ras-related protein Rab-25 (RAB25), Galectin 1 and 12 (LGALS1 and 12) and Profilin-1 (PFN1)

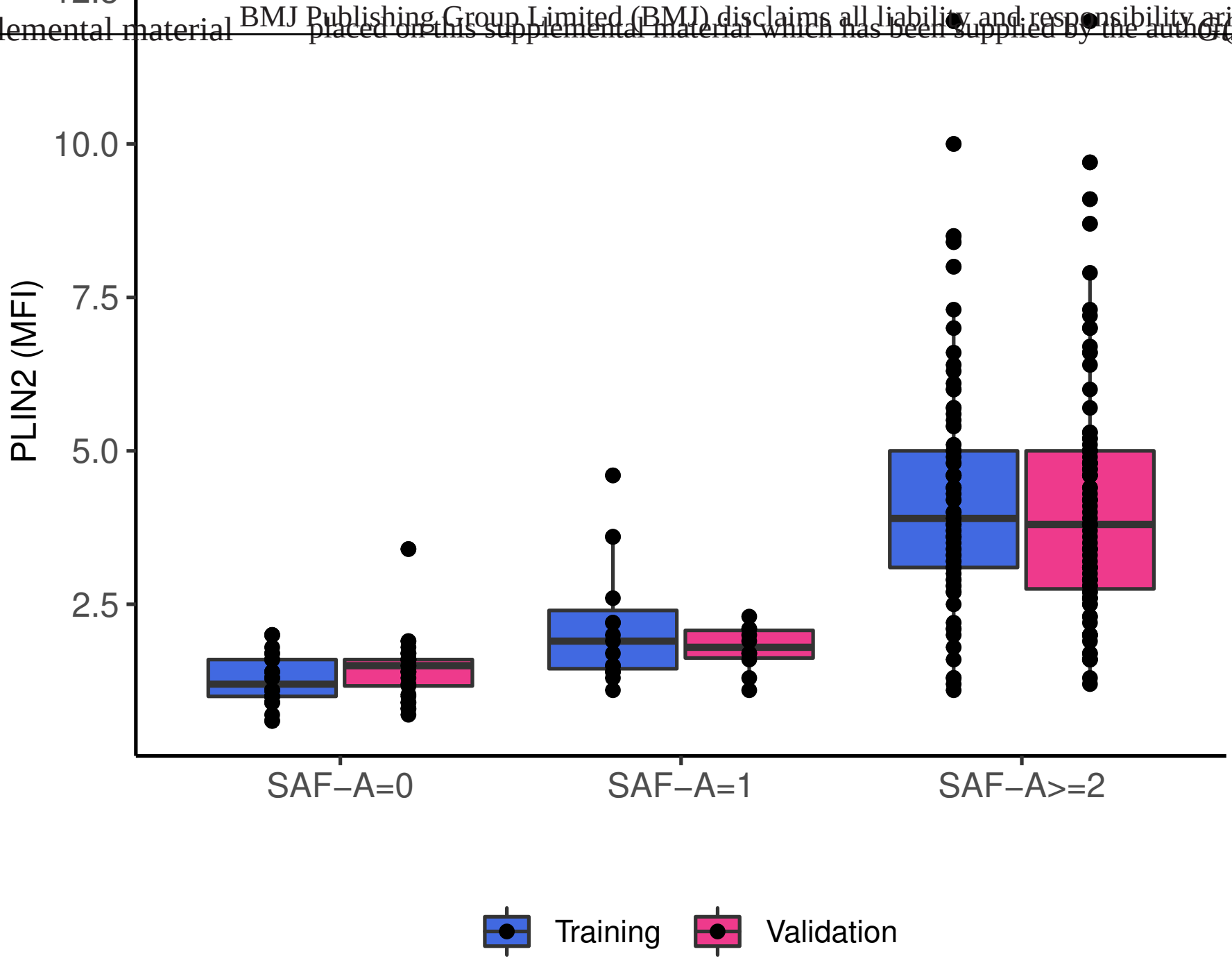
PLIN2 (MFI)
10.0
7.5
5.0
2.5
SAF−A=0
SAF−A=1
SAF−A>=2
Training
Validation

Supplemental Figure 2

Whisker plots of monocyte PLIN2 levels (MFI) measured by flow cytometry in the training and validation cohorts at different levels of SAF-A.

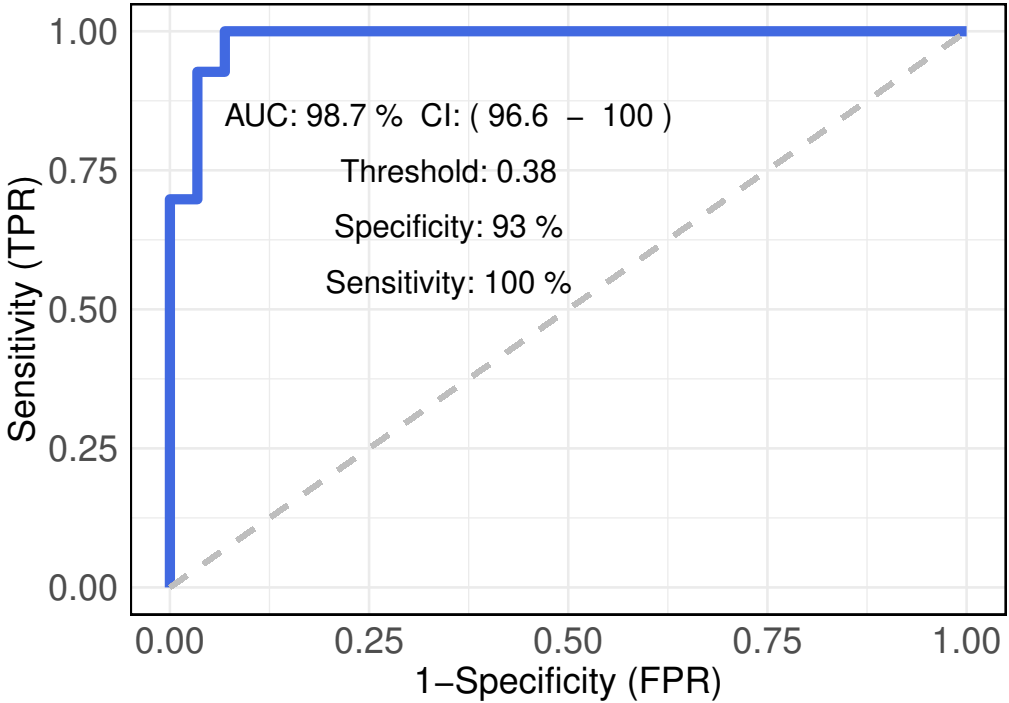
ROC curve
AUC: 98.7 % CI: (96.6 – 100)
Threshold: 0.38
Specificity: 93 %
Sensitivity: 100 %
Sensitivity (TPR)
1−Specificity (FPR)
0.00
0.25
0.50
0.75
1.00

Supplemental Figure 3

ROC curve of PLIN2 algorithm for predicting absence/presence of inflammation (SAF-A=0 vs SAF-A>=1) with the identified threshold, AUROC, sensitivity, and specificity.

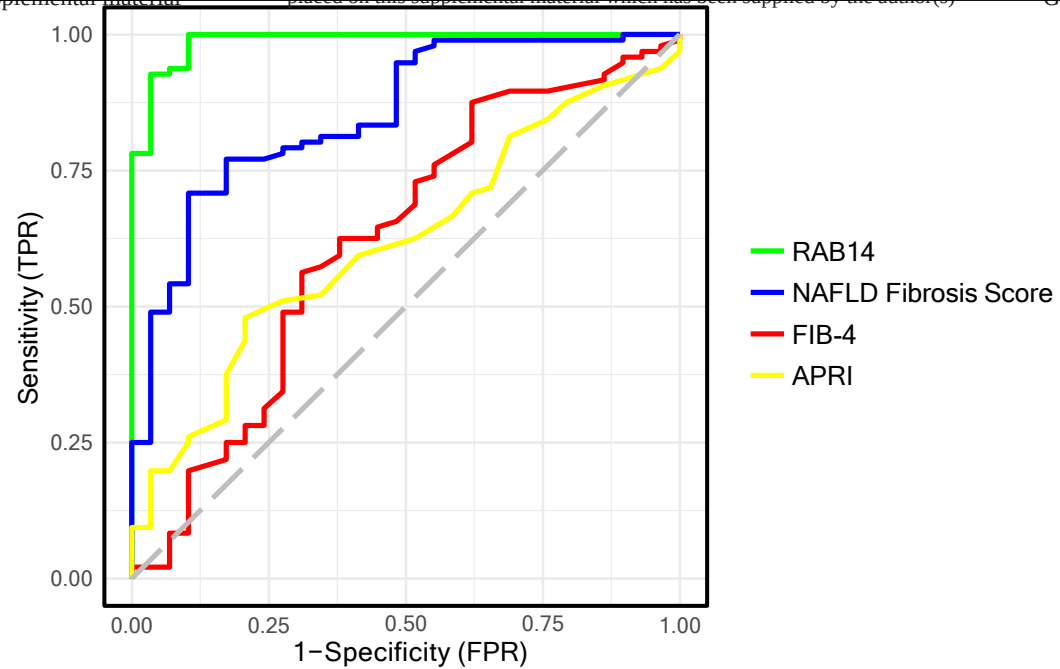
ROC curve
Sensitivity (TPR)
1−Specificity (FPR)
0.00
0.25
0.50
0.75
1.00
RAB14
NAFLD Fibrosis Score
FIB-4
APRI

Supplemental Figure 4

ROC curves for predicting presence/absence of liver fibrosis using the RAB14 algorithm, NAFLD Fibrosis Score, Fibrosis-4 (FIB-4) and AST-to-Platelet Ratio Index (APRI).

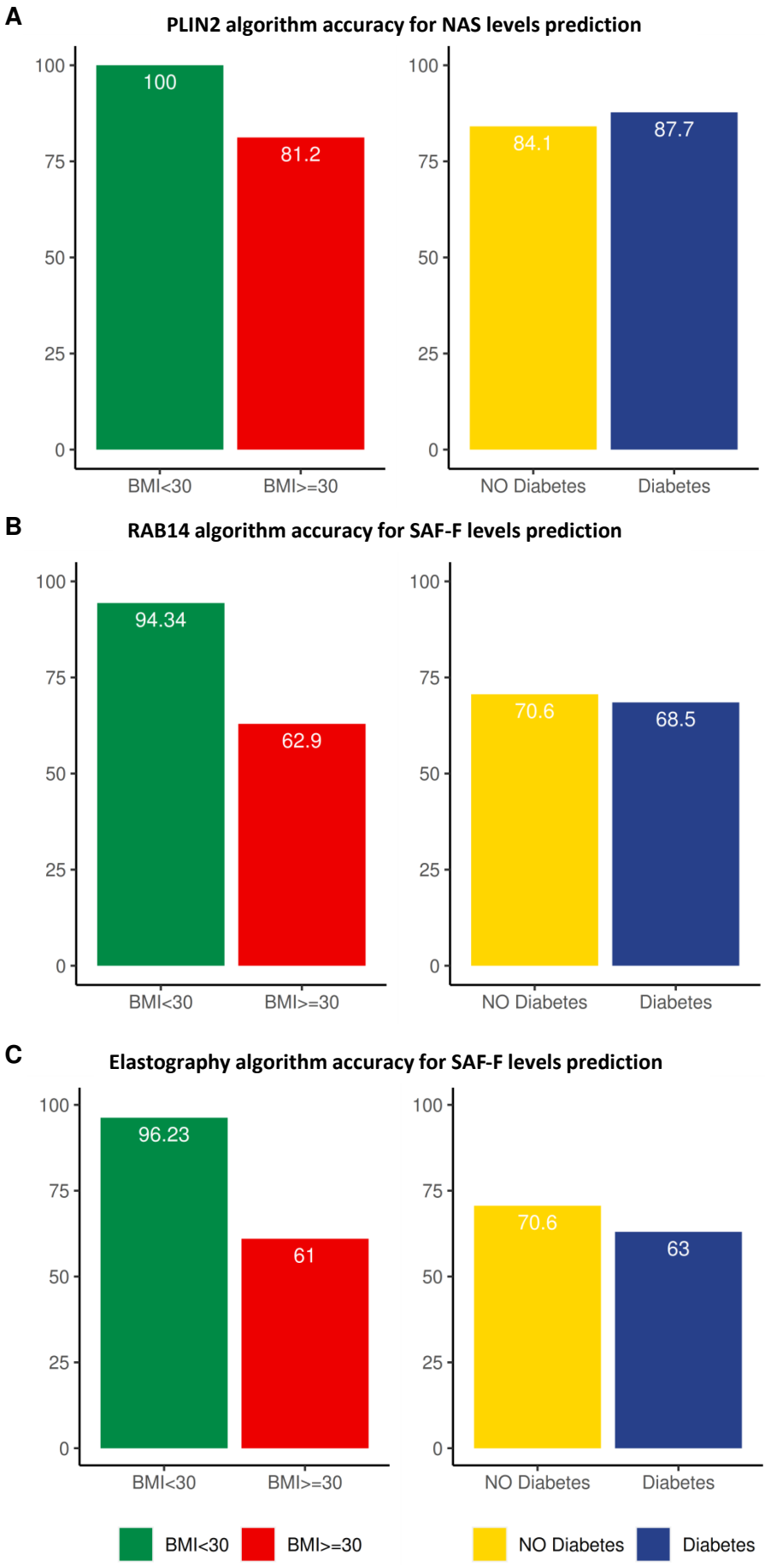
A
PLIN2 algorithm accuracy for NAS levels prediction
100
81.2
84.1
87.7
BMI<30
BMI>=30
NO Diabetes
Diabetes
B
RAB14 algorithm accuracy for SAF-F levels prediction
94.34
62.9
70.6
68.5
C
Elastography algorithm accuracy for SAF-F levels prediction
96.23
61
70.6
63
0
25
50
75
100
BMI<30
BMI>=30
NO Diabetes
Diabetes

Supplemental Figure 5

A: PLIN2 algorithm accuracy for NAS level prediction in subjects with BMI<30 or BMI≥30 (left panel) and in subjects with or without type 2 diabetes (right panel).

B: RAB14 algorithm accuracy for SAF-F level prediction in subjects with BMI<30 or BMI≥30 (left panel) and in subjects with or without type 2 diabetes (right panel).

C: Elastography algorithm accuracy for SAF-F level prediction in subjects with BMI<30 or BMI≥30 (left panel) and in subjects with or without type 2 diabetes (right panel).

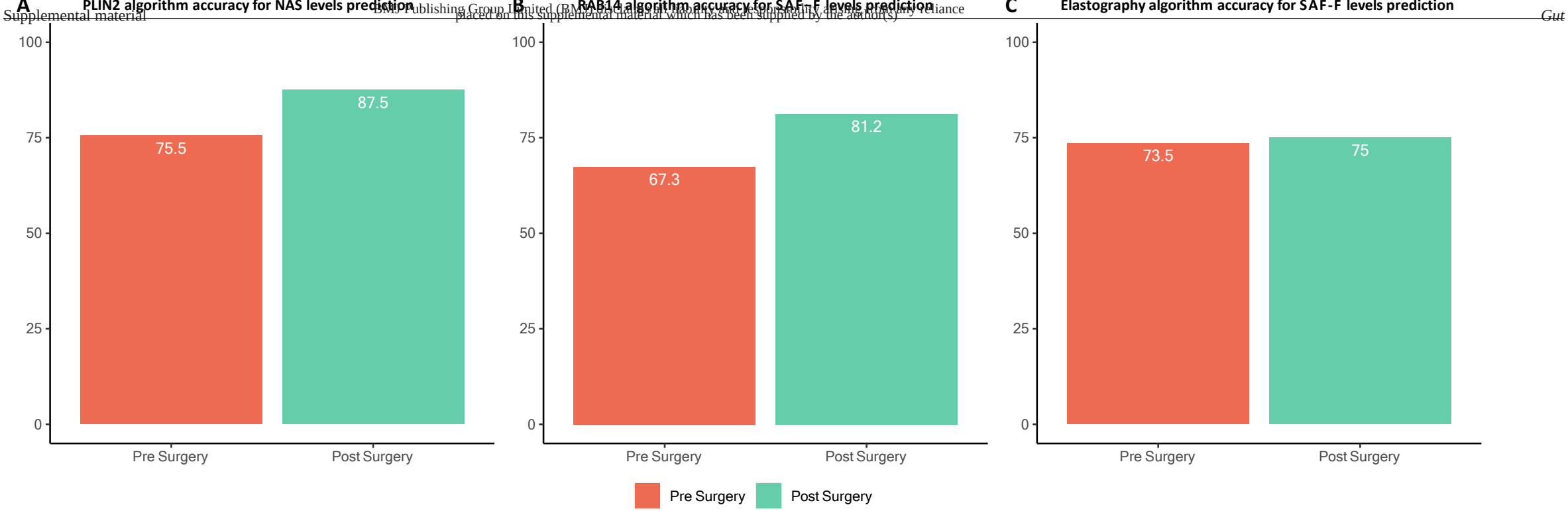
A
PLIN2 algorithm accuracy for NAS levels prediction
B
RAB14 algorithm accuracy for SAF-F levels prediction
C
Elastography algorithm accuracy for SAF-F levels prediction
100
75
50
25
0
75.5
87.5
67.3
81.2
73.5
75
Pre Surgery
Post Surgery
Pre Surgery
Post Surgery

Supplemental Figure 6

A: PLIN2 algorithm accuracy for NAS level prediction in subjects before and after surgery.

B: RAB14 algorithm accuracy for SAF-F level prediction in subjects before and after surgery.

C: Elastography algorithm accuracy for SAF-F level prediction in subjects before and after surgery.

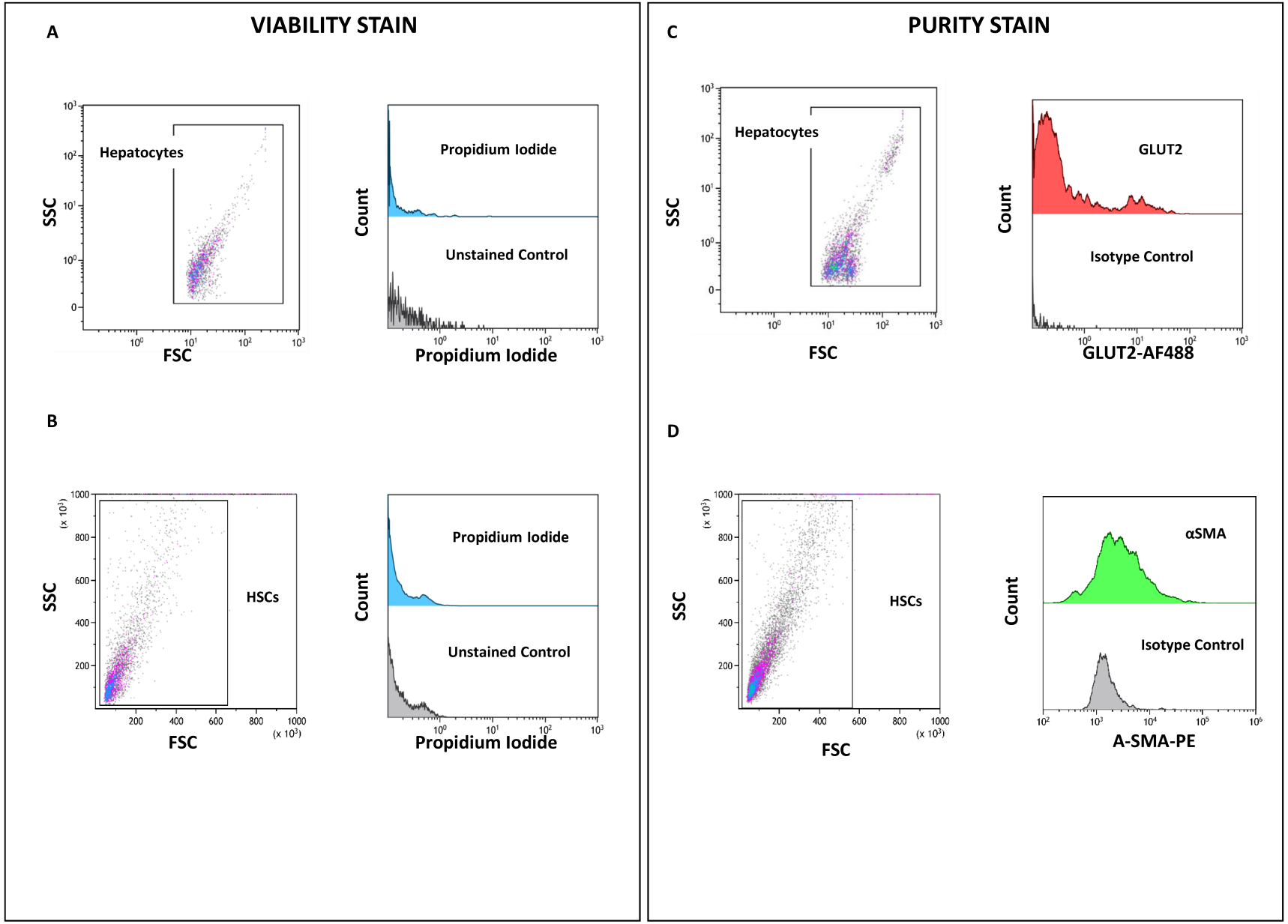
A
VIABILITY STAIN
Hepatocytes
SSC
FSC
Propidium Iodide
Unstained Control
Count
Propidium Iodide
B
HSCs
SSC
FSC
(x 10³)
Propidium Iodide
Unstained Control
Count
Propidium Iodide
C
PURITY STAIN
Hepatocytes
SSC
FSC
GLUT2
Isotype Control
Count
GLUT2-AF488
D
HSCs
SSC
FSC
(x 10³)
αSMA
Isotype Control
Count
A-SMA-PE

Supplemental Figure 7

Cell viability of hepatocytes (A) and hepatic stellate cells (B), stained with propidium iodide and analyzed by flow cytometry.

Cell purity assessed by flow cytometry; primary hepatocytes (C) were stained with GLUT2 Alexa Fluor® 488-conjugated antibody and hepatic stellate cells (D) with α-Smooth Muscle Actin PE-conjugated antibody.

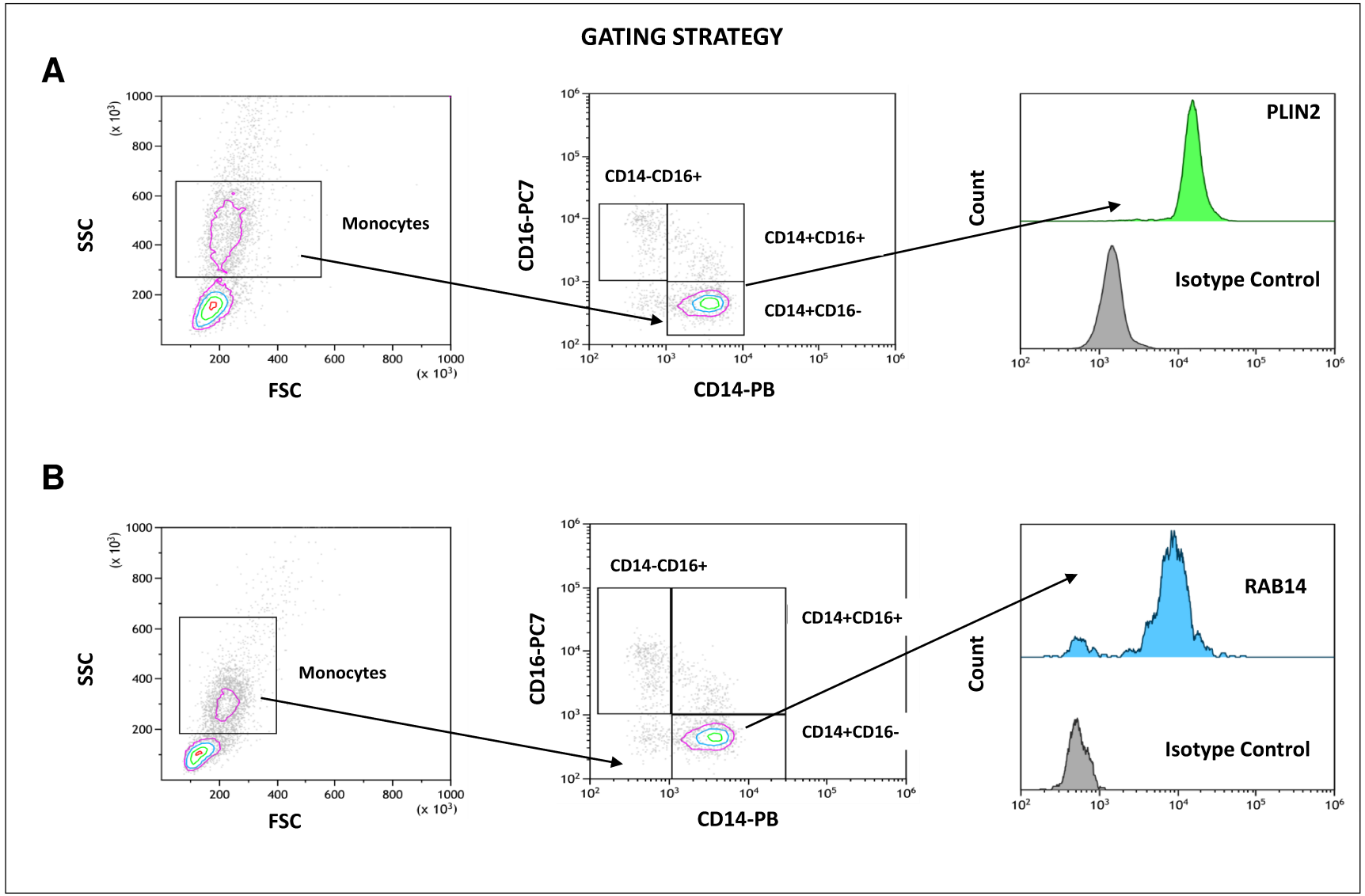
GATING STRATEGY
A
SSC
(x 10³)
FSC
Monocytes
CD16-PC7
CD14-PB
CD14-CD16+
CD14+CD16+
CD14+CD16-
Count
PLIN2
Isotype Control
B
SSC
FSC
Monocytes
CD16-PC7
CD14-PB
CD14-CD16+
CD14+CD16+
CD14+CD16-
Count
RAB14
Isotype Control

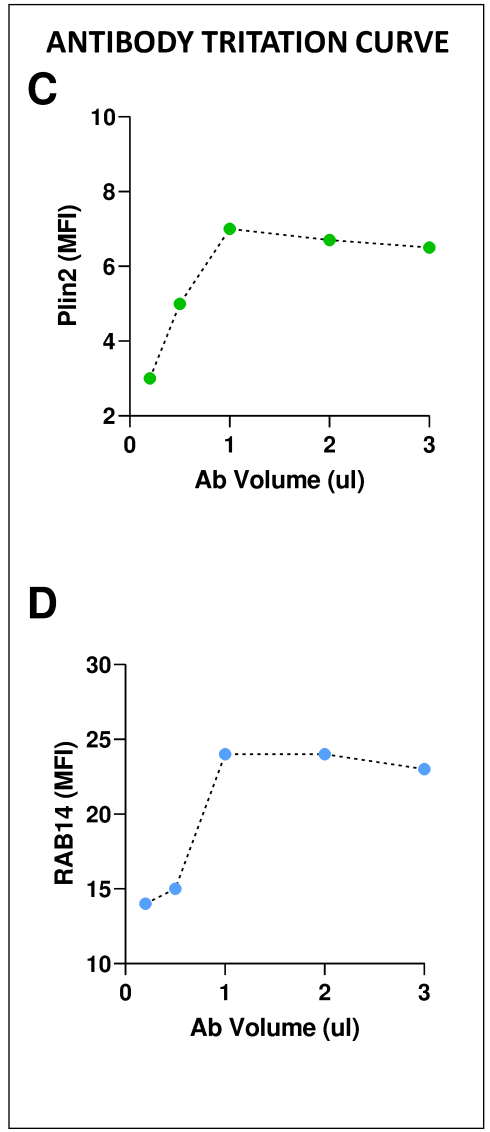
ANTIBODY TRITATION CURVE
C
Plin2 (MFI)
Ab Volume (ul)
D
RAB14 (MFI)
Ab Volume (ul)

Supplemental Figure 8

Gating strategies for PBMCs stained with PLIN2 (A) or RAB14 (B). Antibody tritation curve for PLIN2 (C) or RAB14 (D).

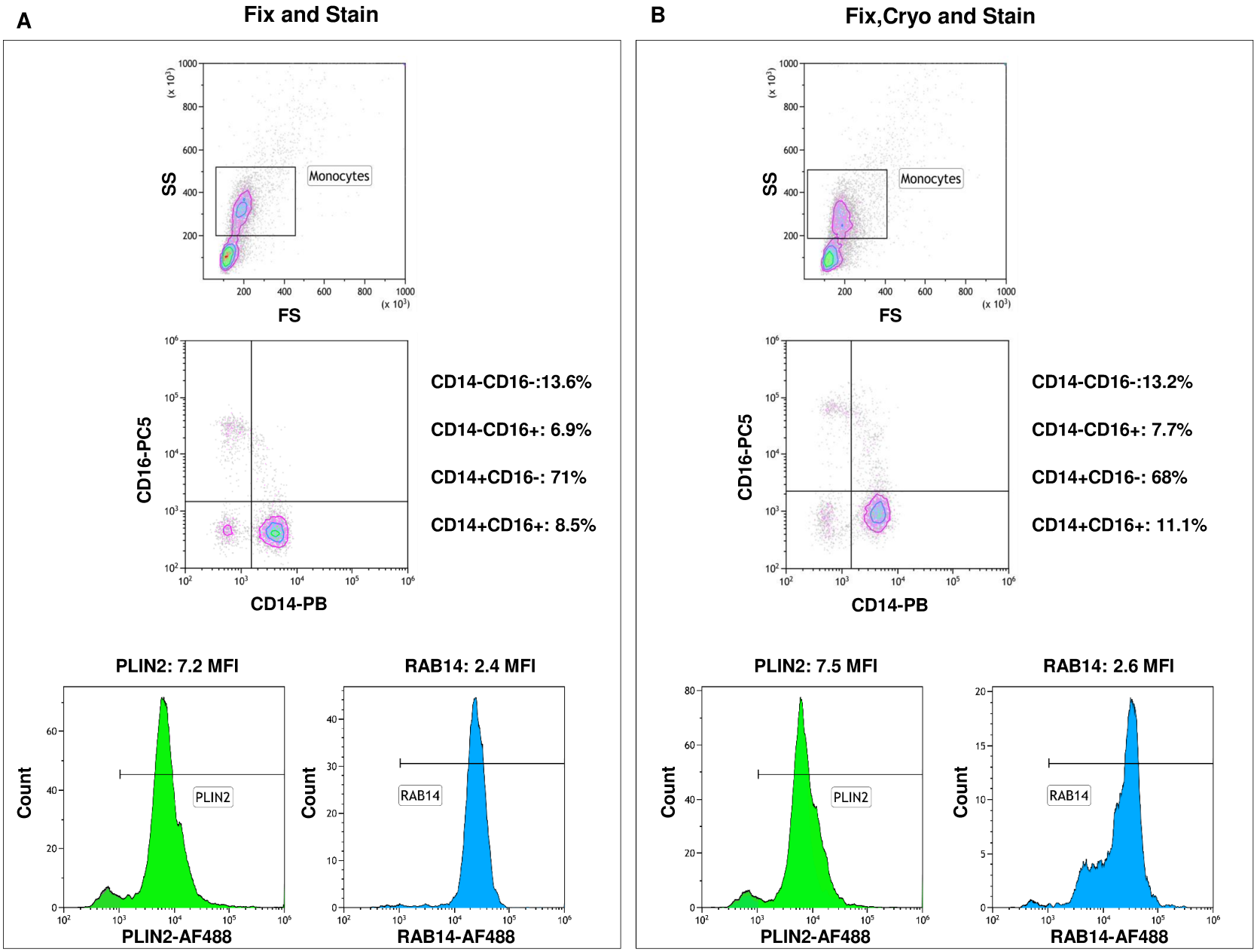
A
Fix and Stain
B
Fix,Cryo and Stain
Monocytes
SS
FS
CD16-PC5
CD14-PB
CD14-CD16-:13.6%
CD14-CD16+: 6.9%
CD14+CD16-: 71%
CD14+CD16+: 8.5%
CD14-CD16-:13.2%
CD14-CD16+: 7.7%
CD14+CD16-: 68%
CD14+CD16+: 11.1%
PLIN2: 7.2 MFI
RAB14: 2.4 MFI
PLIN2: 7.5 MFI
RAB14: 2.6 MFI
Count
PLIN2
RAB14
PLIN2-AF488
RAB14-AF488

Supplemental Figure 9

Influence of the different handling procedures on PBMCs stained for PLIN2 or RAB14. Cells were processed using the following procedures: fixation and staining (A) or fixation, cryopreservation and staining (B).

SUPPLEMENTAL MATERIALS

Antropometric measures

Height and weight were measured and body mass index (BMI) calculated as weight (kg)/stature $(m)^2$. Waist circumference was measured at the part of the trunk midway between the most caudal part of the lateral costal arch and the iliac crest in the morning before breakfast, after lavatory visit with the person standing with feet about 25-30 cm apart. The circumference was measured to the nearest 0.5 cm, at the end of a normal expiration. Hip circumference was measured as the maximal circumference over the buttocks.

Dual X-Ray Absorptiometry

Body composition was assessed by dual X-ray absorptiometry (DEXA), using a Lunar DPX-L scanner (Lunar Corporation, WI, USA). Scanning mode was determined from the body mass index by the scanner software (version 1.3).

Blood samples analyses

Peripheral blood samples were drawn at 8:00 a.m. after an overnight fast. Plasma glucose, glycated hemoglobin (HbA1c), transaminases, γGlutamyl transferase, lipid profile and blood count were measured by routine analysis. Insulin was measured by ARCHITECT Insulin assay (Abbott Laboratories), a chemiluminescent microparticle immunoassay (CMIA).

Proteomics

Monocytes, isolated from 3 mL of heparinized blood, or HSC obtained from liver biopsies, were mixed with lysis buffer, containing 100µL of 5mM Tris-HCl buffer at pH 8.0, 0.1M Triton X-100 and protease inhibitor cocktail, for 30 minutes on ice. Cell lysates were centrifuged at 4˚C for 10 minutes at 1,500 rpm. Supernatants were stored in aliquots at -80˚C until analyses and pellet discharged. Pierce™ BCA Protein Assay Kit measured the protein concentrations. One-hundred µg of protein per sample were digested by filter-aided sample preparation (1).

Trypsin-catalyzed 16O/18O labelling was performed according to Qian et al. (2) and Petritis et al. (3) iTRAQ labelling was performed using the reagents and protocols supplied in the 8Plex Multiplex kit. Each dried iTRAQ-labelled peptide sample was dissolved in 15 µl of 0.1% ammonium formate and then separated by nano-LC-MS/MS using an Eksigent ekspert TM nano-LC 425 system coupled with a TripleTOF 6600 System (SCIEX). Peptides were eluted at a flow rate of 300 nl/min into a reverse phase C18 column using a linear gradient of acetonitrile (3–36%) in 0.1% formic acid with a running time of 120 minutes. Mass spectra and tandem mass spectra were recorded. The nanospray needle voltage was 2,300 V. The mass window for precursor ion selection of the quadrupole mass analyzer was ±2 m/z. We used Proteome Discoverer 1.4 with the SEQUEST algorithm to search the original MS/MS protein data in the specified non-redundant databases. The differential protein abundance in monocytes and in HSCs between liver fibrosis and absence of liver fibrosis was calculated by ANOVA. Q values were computed adjusting the p-values found using an optimized False Discovery Rate (FDR) approach with parameters set with a strict target FDR at <0.0001 (4).

Human Primary hepatocytes isolation

Hepatocytes from obese, NAFLD subjects and healthy subjects were processed and collected in an icebox at 4 °C under aseptic conditions, as described elsewhere (5). Tissue obtained during percutaneous liver biopsy, approximatively 3 cm length, 2 cm were diced into smaller pieces, <3 mm each, and washed in HBSS to remove excess blood. Tissue was then transferred to a tube containing pre-warmed EGTA buffer (HBSS, 0.5 mM EGTA, 0.5% fatty acid free bovine serum albumin (BSA)) and agitated (100 rpm) in a water bath with shaking bed for 10 min, 37 °C. After three washes, to remove the remaining blood and EGTA, the tissue was placed in pre-warmed digestion buffer (HBSS, 0.05% collagenase IV, 0.5% fatty acid free BSA, 10 mM CaCl2) and agitated (100 rpm) in a water bath with shaking bed for 30 min, 37 °C. The digested tissue was filtered through 100 µm cell strainer while the remaining tissue

was again digested in fresh digestion buffer. Cell suspensions were pooled and centrifuged at 80 g for 5 min, 4 °C and the supernatant discarded. Cells were grown on cover slips until confluent and used for immunofluorescence analysis or directly stained with PLIN2 for flow cytometry analysis.

Human Primary Hepatic Stellate cells isolation

Hepatic stellate cells from obese, NAFLD subjects and healthy subjects were isolated from resected liver human tissue as described elsewhere (6). Briefly, liver biopsy was placed in a Petri dish, washed 5 times with a sterile phosphate-buffered saline (PBS) solution to remove residual blood from the tissue surface and finely minced into small pieces of less than 3 mm each. The liver was then digested using pronase and collagenase solution (Merck, Darmstadt, DE) followed by density gradient centrifugation (1,380g for 17 min at 4 °C without brake) using Nicodenz (Merck, Darmstadt, DE) to remove non-parenchymal cells. Isolated cells were grown on cover slips until confluence and used for immunofluorescence or directly stained with RAB14 for flow cytometry analysis.

Cell viability and cell purity after isolation

To assess cell viability, hepatocytes and hepatic stellate cells were stained with propidium iodide and analyzed by flow cytometry. Cell purity was assessed by flow cytometry by staining primary hepatocytes with GLUT2 Alexa Fluor® 488-conjugated antibody and hepatic stellate cells with α-Smooth Muscle Actin PE-conjugated antibody. Flow cytometry analysis for both primary hepatocytes and hepatic stellate cells are reported in supplemental figure 7 A-D.

Isolation of Peripheral Blood Mononuclear Cells

Blood (3 ml) from subjects with obesity and NAFLD and from healthy subjects, was collected using EDTA as an anticoagulant and processed within 2 hours. Peripheral blood mononuclear cells (PBMCs) were obtained from whole blood by standard gradient centrifugation over lympholyte®-h cell separation media. In brief, blood was diluted 1:1 (vol/vol) in PBS, carefully

layered on lympholyte®-h cell separation media and centrifuged at room temperature for 25 min at 1,600 × g. PBMCs were washed, resuspended in PBS and used for flow cytometry. CD14+CD16- monocytes were isolated from PBMCs using classical monocyte isolation kit, following manufacturer's instruction. Using a cyto-centrifuge (Hettich, Tuttlingen, DE), cells were deposited on the slides and used for immunofluorescence analysis.

Immunofluorescence

Nile red staining of neutral lipids was used to identify lipid droplets accumulation in primary hepatocytes. Hepatocytes were fixed in 4% paraformaldehyde for 10 min at room temperature and stained with Nile Red (100 ng/mL) for 10 minutes at room temperature. Nuclear staining was performed with DAPI. PLIN2 staining was performed on primary hepatocytes and monocytes, while RAB14 staining was performed on primary HSCs and monocytes. Cells were fixed in 4% paraformaldehyde for 10 min at room temperature, permeabilized with PBS containing 0.1% Triton X-100 and blocked with 1% BSA. Primary antibodies were incubated overnight at 4 °C while secondary antibodies were incubated for 1 hour at room temperature in the dark. Nuclear staining was performed with DAPI and slides were mounted on ProlongGold.

Flow Cytometry

All flow cytometry data were acquired on 9-color/3-laser Cytoflex flow cytometers (Beckman Coulter, Brea, CA) and were analyzed with Kaluza software (Beckman Coulter, Brea, CA). CytoFLEX Daily QC beads were run as quality control to verify optical alignment and fluidics system. Fluorescence target channels were met for all channels by using CytoFLEX Daily QC beads as well, and the acquisition settings were defined by using VersaComp Antibody Capture Kit.

Gating strategies for both primary hepatocytes and PBMCs are reported in supplemental figure 8 A,B. The technician doing flow cytometry measurements was blinded to the sample identity.

The levels of PLIN2 and RAB14 in monocytes are reported as Median Fluorescence intensity (MFI). MFI represents the number of antibodies that recognize and attach to the cell antigens, allowing the exact quantification of antigen expression per cell.

Validation parameters

All validation procedures, unless specified otherwise, were performed on PBMCs (1x106 cells/ml) from subjects with obesity and NAFLD (N=3), following the standard operating procedures (SOP). Conventional sample acceptance criteria include non-hemolyzed and unclotted conditions. Assay reproducibility and stability as well as limit of detention and quantification are reported in online supplemental table 7.

Intra-assay precision (repeatability)

Each sample was processed in triplicate and run one time. Samples were processed and assayed on the same day to avoid the influence of sample instability. For the statistical evaluation, the mean of %CV was calculated for all samples (Mean %CV) and the intra-assay precision described as the Mean %CV.

Inter-assay precision (reproducibility)

Each sample was processed in triplicate and run two times. Samples were processed and assayed on the same day to avoid the influence of sample instability. Since the inter-assay samples were run on the same day, every effort was made to guarantee that the runs were independent of each other. Indeed, we have performed, for each analytical run, separate sample processing and acquisition. For the statistical evaluation, the mean of the %CV was calculated for each sample (Mean %CV) and the inter-assay precision was reported as the Mean %CV.

Lower limit of blank/detection

For determine the lower limit of blank/detection we have used a sample partially stained (CD14 staining) by omitting antibodies (Anti-ADFP antibody [EPR3713] (Alexa Fluor® 488) and RAB14 (D-5)). Through this strategy, the antigen of interest will not be detected.

Limit of Quantification

For determine the limit of quantification healthy volunteer (N=3) that minimally express the antigen of interest were used.

Antibody Tritation Curve

Antibody tritation was performed to identifying the correct concentration of antibody, to ensure the antibody performs within acceptable parameters and to eliminate nonspecific antibody binding. Serial concentrations (0.0625 µg/µl, 0.125 µg/µl, 0.25 µg/µl, 0.5 µg/µl and 1 µg/µl) of Anti-ADFP antibody [EPR3713] (Alexa Fluor® 488) were used to stain the samples. Serial concentrations (0.04 µg/µl, 0.1 µg/µl, 0.2 µg/µl, 0.4 µg/µl, and 0.6 µg/µl) of RAB14 (D-5), conjugated with Alexa Fluor® 488 secondary antibody, were used to stain the samples. Antibody tritation curves are reported in supplemental figure 8 C,D.

Cryopreservation of PBMCs

PBMCs were fixed for 45 min and then immediately stored at -80°C. Cells were thawed rapidly in a water bath at 37°C, washes and resuspended in PBS 1X. Staining for PLIN2, RAB14 CD14 and CD16 are reported in supplemental figure 9 A,B.

Reagents

We have provided a detailed list of reagents in online supplemental Table 8.

STATISTICS

We aimed to verify whether our biomarker predicted SAF-A levels. The whole dataset was split into a discovery and a validation sample with an equal number of subjects with NASH according to the SAF-A values; absence of NASH if SAF-A=0; presence of NASH if SAF-A≥1.

First, we tested those variables in addition to PLIN2 that were representative of metabolic, lipidic, and hepatic profiles, and were predictive of SAF-A, using a univariate analysis (Supplemental Table 1). We then assessed in a multivariate logistic model whether PLIN2 MFI, waist circumference, age, plasma glucose, triglycerides and ALT were accurate in predicting the presence (SAF-A≥1) or absence (SAF-A=0) of histologic activity. A stepwise elimination procedure was applied to find the subset of predictors, resulting in the best performing model. The variables entering the final model were PLIN2, waist circumference, glycemia and age (Supplemental Table 2).

Then, we ascertained whether our algorithm was able to predict the severity of SAF-A. For this purpose, the SAF-A score was recoded as a 3-level variable: SAF-A_level=0 if SAF-A=0; SAF-A_level=1 if SAF-A=1; and SAF-A_level=2 if SAF-A≥2 and a multinomial model, including only significant predictors in a stepwise regression, used.

REFERENCES

1. Wiśniewski JR, Zougman A, Nagaraj N, et al. Universal sample preparation method for proteome analysis. *Nat Methods* 2009;6:359-362.
2. Qian WJ, Monroe ME, Liu T et al. Quantitative Proteome analysis of human plasma following in vivo lipo-polysaccharide administration using16O/18O labeling and the accuratemass and time tag approach. *Mol Cell Proteomics* 2005;4:700-709.
3. Petritis K, Kangas LJ, Ferguson PL. Use of artificial neural networks for the prediction of peptideliquid chromatography elution times in proteome analyses. *Anal Chem* 2003;75:1039-1048.
4. Savitski MM, Wilhelm M, Hahne H, et al. A Scalable Approach for Protein False Discovery Rate Estimation in Large Proteomic Data Sets. *Mol Cell Proteomics* 2015;14:2394-2404.
5. Green CJ, Charlton CA, Wang LM, et al. The isolation of primary hepatocytes from human tissue: optimising the use of small non-encapsulated liver resection surplus. *Cell Tissue Bank* 2017;18:597-604.
6. Zhai X, Wang W, Dou D, et al. A novel technique to prepare a single cell suspension of isolated quiescent human hepatic stellate cells. *Sci Rep* 2019;9:12757. doi:10.1038/s41598-019-49287-7.

Supplemental Table 1. Results from the univariable logistic model for SAF-A prediction (presence/absence)

Variable	Beta coefficient	P value
PLIN2 (MFI)	2.774	3.25E-05
Waist circumference (cm)	0.120	3.03E-08
AST/Platelet index	3.690	0.100
Gender (male = 1)	0.020	0.963
Diabetes (presence = 1)	3.020	0.004
Age (years)	0.210	4.95E-08
BMI (kg/m^2)	0.312	1.61E-08
Hips Circumference (cm)	0.164	7.87E-07
HDL (mg/dl)	-0.038	0.001
LDL (mg/dl)	0.011	0.083
Triglycerides (mg/dl)	0.0278	0.0001
Cholesterol (mg/dl)	0.016	0.026
Glycemia (mg/dl)	0.101	7.13E-06
Insulinemia (IU/ml)	0.539	5.29E-05
HOMA-IR ((μIU/mL)(mmol/L)/22.5)	2.573	1.86E-05
AST (IU/l)	0.168	0.0003
ALT (IU/l)	0.145	4.84E-05
GGT (IU/l)	0.085	0.0017

In bold the variables that were tested in a multivariable model and that were chosen as representative of the metabolic (glycemia), lipidic (triglycerides) and hepatic profiles (ALT) along with PLIN2 (MFI), waist circumference and age

Supplemental Table 2. Final multivariable logistic model after a step regression procedure for SAF-A prediction (presence/absence)

Variable	Beta coefficient	P value
Intercept	-75.040	0.0015
PLIN2 (MFI)	2.971	0.0152
Waist circumference (cm)	9.028	0.0063
Age (years)	8.708	0.0034
ALT (IU/l)	0.145	4.84E-05

All variables were log-transformed

Supplemental Table 3. Classes of drugs used for diabetes, hypertension and hyperlipidemia treatment in the discovery and validation cohorts

	Discovery Cohort	Validation Cohort
Anti-Diabetes Medications		
SGLT2 inhibitors	60%	60%
GLP1 RAs	30%	35%
Pioglitazone	40%	45%
DPP IV inhibitors	10%	5%
Metformin	100%	100%
Anti-Hypertension Medications		
Beta-blockers	65%	60%
ACE inhibitors	70%	70%
Angiotensin II receptor blockers	30%	40%
Calcium channel blockers	15%	20%
Anti-Hyperlipidemic Medications		
Statins (Atorvastatin)	80%	75%
Cholesterol Absorption Inhibitors (Ezetimibe)	20%	25%

Percentage of patients using a specific class of drugs among those with T2D, hypertension and hyperlipidemia.

Supplemental Table 4. Final multinomial logistic model after a step regression procedure for SAF-A level prediction (SAF-A_level=0 if SAF-A=0; SAF-A_level=1 if SAF-A=1; and SAF-A_level=2 if SAF-A≥2)

Variable		Beta coefficient	P value
Intercept	level 1	-59.83898	0.015
	level 2	-71.00549	0.003
PLIN2 (MFI)	level 1	0.03320633	0.984
	level 2	4.24301361	0.005
Waist circumference (cm)	level 1	11.904624	0.012
	level 2	9.314543	0.032
Age (years)	level 1	8.215290	0.007
	level 2	7.477506	0.009
Glycemia (mg/dl)	level 1	-5.9964274	0.194
	level 2	-0.5078786	0.907

Supplemental Table 5. Results from the univariable logistic model for SAF-F prediction (presence/absence)

Variable	Beta coefficient	P value
RAB14 (ng/ml)	-0.09796	0.001042
Elastography	2.38349	4.88E-06
Waist circumference (cm)	0.153981	1.36E-06
Gender (male = 1)	0.212175	0.653057
Diabetes (presence = 1)	17.53943	0.98749
Age (years)	0.170324	4.62E-07
BMI (kg/m^2)	0.405609	1.14E-06
Hips Circumference (cm)	0.514379	0.010899
HDL (mg/dl)	-0.05248	0.000168
LDL (mg/dl)	0.014881	0.045473
Triglycerides (mg/dl)	0.024294	0.000229
Cholesterol (mg/dl)	0.011876	0.102235
Glycemia (mg/dl)	0.112788	1.10E-05
Insulinemia (IU/ml)	0.230373	0.000296
HOMA-IR ((μIU/mL)(mmol/L)/22.5)	1.041393	0.00011
AST (IU/l)	0.119634	0.005087
ALT (IU/l)	0.117491	0.000433
GGT (IU/l)	0.019475	0.130297

In bold the variables that were tested in a multivariable model and that were chosen as representative of the metabolic (glycemia), lipidic (HDL) and hepatic profiles (ALT) along with Rab14 or Elastography, waist circumference and age

Supplemental Table 6. Multinomial logistic model for SAF-F level prediction (SAF-F_level=0 if SAF-F=0; SAF-F_level=1 if SAF-F=1; and SAF-F_level=2 if SAF-F≥2) for individuals who underwent surgery procedure

Variable		Beta coefficient	P value
Intercept	level 1	60.61844	0.274
	level 2	30.86940	0.608
RAB14 (ng/ml)	level 1	-12.17215	0.110
	level 2	-15.95249	0.040
Waist circumference (cm)	level 1	-12.98499	0.273
	level 2	-12.31895	0.314
Age (years)	level 1	8.537065	0.211
	level 2	12.042225	0.114
Glycemia (mg/dl)	level 1	-0.2664244	0.959
	level 2	0.9475479	0.878
HDL (mgdl)	level 1	1.489295	0.426
	level 2	4.846866	0.085
ALT (IU/l)	level 1	-0.4477087	0.811
	level 2	0.3593118	0.867

Supplemental Table 7. Assay Reproducibility and Sensitivity

	PLIN2	**RAB14**
Intra-Assay Precision (%)	9.2	5.1
Inter-Assay Precision (%)	9.5	2.3
Limit of Detection (MFI)	0.43±0.02	0.55±0.01
Lower limit of blank (MFI)	0.7±0.05	0.8±0.02

Supplemental Table 8. List of reagents

REAGENT or RESOURCE	SOURCE	IDENTIFIER
Human Glut2 Alexa Fluor® 488-conjugated Antibody	R&D Systems, Minneapolis, NE	FAB1414G
Human alpha-Smooth Muscle Actin PE-conjugated Antibody	R&D Systems, Minneapolis, NE	IC1420P
CD14-Pacific Blue	Beckman Coulter, Brea, CA	B00846
CD16-Phycoerythrin/Cyanin 7	Beckman Coulter, Brea, CA	6607118
Anti-ADFP antibody [EPR3713] (Alexa Fluor® 488)	Abcam, Cambridge, UK	ab201535
Goat Anti-Mouse IgG, Alexa Fluor® 488	Merk, Darmstadt, DE	SAB4600387
RAB14 (D-5)	Santa Cruz Biotechnology, Dallas, TX	sc-271401
Goat anti-Mouse IgG, Alexa Fluor® 568	Thermo Scientific, Waltham, MA	A-11031
Tris-HCl	Sigma-Aldrich, St. Louis MO	10812846001
Triton X-100	Merk, Darmstadt, DE	11754599001
Halt™ Protease Inhibitor Cocktail (100X)	Thermo Scientific, Waltham, MA	78429
Ammonium formate	Sigma-Aldrich, St. Louis MO	70221
Formic acid	Sigma-Aldrich, St. Louis MO	F0507
Hanks' Balanced Salt Solution (HBSS)	Merk, Darmstadt, DE	1.00496
EGTA	Merk, Darmstadt, DE	E3889
Fetal Bovine Serum	Thermo Scientific, Waltham, MA	16000044
Collagenase IV	Thermo Scientific, Waltham, MA	17104019
Pronase	Merk, Darmstadt, DE	10165921001
Lympholyte®-h cell separation media	Cedarlane Lab, Burlington, CA	CL5010
Phosphate-buffered saline	Thermo Scientific, Waltham, MA	10010023
4% paraformaldehyde solution	Merk, Darmstadt, DE	HT501128
Nile Red	Thermo Scientific, Waltham, MA	N1142
DAPI	Thermo Scientific, Waltham, MA	D1306
ProLong™ Gold Antifade	Life Technologies, Carlsbad, CA	P36931
ARCHITECT Insulin assay	Abbott Laboratories, Chicago, IL	8K41
Pierce™ BCA Protein Assay Kit	Thermo Fisher Scientific, Waltham,MA	23225
iTRAQ® Reagent - 8PLEX Multiplex Kit	Sigma-Aldrich, St. Louis MO	4381663
Classical Monocyte Isolation Kit, human	Miltenyi Biotec, Bergisch Gladbach,DE	130-117-337
CytoFLEX Daily QC beads	Beckman Coulter, Brea, CA	B53230
VersaComp Antibody Capture Kit	Beckman Coulter, Brea, CA	B22804